

INVESTIGATION OF THE BUCKLING BEHAVIOUR  
OF CIRCUMFERENTIALLY WELDED PIPELINES

JOHN BARRETT







**INVESTIGATION OF THE BUCKLING BEHAVIOUR  
OF CIRCUMFERENTIALLY WELDED PIPELINES**

**by**

**© John Barrett**

**A thesis submitted to the  
School of Graduate Studies  
in partial fulfillment of the  
requirements for the degree of  
Master of Engineering**

**Faculty of Engineering and Applied Science  
Memorial University of Newfoundland**

**May 2009**

**St. John's**

**Newfoundland**

**Canada**

## **ABSTRACT**

Many researchers have studied the buckling behaviour of pipelines under combined loading in the interest of defining pipeline capacity as the pipe undergoes large deformation due to extreme ground movement. Past studies have used a number of physical, analytical, and numerical methods in order to understand pipeline behaviour and define the strain limits necessary in limit states design. A review of published works has been presented here as well as two conference papers detailing the calibration of a numerical model and comments on the buckling behaviour of a pipeline.

The first paper, accepted by OMAE 2009, extensively described the calibration of the numerical model which was used to study the buckling behaviour and capacity of pipelines. This paper had specific interest in the effects of radial offset imperfections, due to girth welding process, on structural capacity. A parametric study also examined diameter, thickness, internal applied pressure and applied axial force. The presence of a compressive axial force was shown to decrease critical moment and strain. Strain capacity was shown to be reduced by as much as 35% depending on the magnitude of girth weld imperfection. Strain behaviour over various pressure levels was shown to be non-linear and shown to be reflected in the development of strain based equations.

The second paper, submitted to CSCE 2009, conducted further analysis on the results generated from the parametric study with a focus on the resultant buckled waveforms and pipeline section ovality. Buckled wavelength and amplitude were influenced by pipeline

diameter, diameter to thickness ( $D/t$ ) ratio and applied internal pressure with limited influence from misalignment amplitude. Ovality, a measure of pipeline out-of-roundness, was found to remain constant over diameter, increase with decreasing  $D/t$ , decrease with internal pressure, and remain unaffected by axial force or amplitude of imperfection. End effects were discovered to be a problem when considering pressurized pipes and have been quantified for select cases. This has been shown to be a direct result of the diameter to length ratio of the tested pipeline. As result, it is recommended that the length to diameter ratios for test sections should be as large as practical, for both numerical and physical tests, to avoid boundary effects.

The numerical procedure developed in this study has shown to be consistent with a number of sources, Ghodsi et al. (1994), Dorey (2001) and Torselletti et al. (2005). The main conclusion and recommendation given as a result of this study was that boundary effects greatly influence the buckling behaviour of the short pipelines studied and that further investigations warrants the use of longer test sections.

## **ACKNOWLEDGEMENTS**

The completion of this document would not have been possible without the help and support of many individuals and the organization C-CORE. I would like to thank C-CORE for the opportunity of pursuing a Master's degree in Engineering. C-CORE's commitment to provided time, monetary support and flexibility to all of its employees to pursue higher education has made this goal possible.

I would like to acknowledge my supervisors, both Dr. Shawn Kenny and Dr. Ryan Phillips, whose guidance and experience has facilitated this research.

I would like to extend my sincere thanks for the moral support provided by my parents, Lewis and Gladys, and brother and sister, Kristopher and Karen. Without their belief in my abilities, I would not have been able to complete this research.

To my wife Catherine, I thank whole heartedly. Her patience, and often tough love, has brought me through this ordeal. Thank you for your support.

## TABLE OF CONTENTS

ABSTRACT.....	ii
ACKNOWLEDGEMENTS.....	iv
LIST OF FIGURES .....	vi
LIST OF ABBREVIATIONS AND SYMBOLS .....	viii
LIST OF APPENDICES.....	x
1. INTRODUCTION, OVERVIEW AND CO-AUTHORSHIP STATEMENT .....	1-1
1.1. INTRODUCTION .....	1-1
1.2. OVERVIEW .....	1-1
1.3. CO-AUTHORSHIP STATEMENT .....	1-2
2. LITERATURE REVIEW .....	2-1
2.1. EXPERIMENTAL AND ANALYTICAL INVESTIGATIONS .....	2-1
2.2. NUMERICAL AND PARAMETRIC INVESTIGATIONS .....	2-3
2.3. PIPELINE DESIGN CODES AND GUIDELINES .....	2-12
2.4. SUMMARY .....	2-15
3. OMAE 2009 – EFFECTS OF GIRTH WELD ON THE LOCAL BUCKLING RESPONSE OF CONVENTIONAL GRADE PIPELINES.....	3-1
3.1. SYNOPSIS.....	3-1
3.2. ABSTRACT.....	3-5
3.3. INTRODUCTION .....	3-6
3.4. CALIBRATION OF NUMERICAL MODEL .....	3-7
3.5. A PARAMETRIC ANALYSIS .....	3-13

3.6.	RESULTS .....	3-15
3.7.	CONCLUSIONS.....	3-19
3.8.	REFERENCES .....	3-22
4.	CSCE 2009 – INVESTIGATION ON THE BUCKLING BEHAVIOUR OF GIRTH WELDED PIPELINES .....	4-1
4.1.	SYNOPSIS.....	4-1
4.2.	ABSTRACT.....	4-2
4.3.	INTRODUCTION .....	4-3
4.4.	CALIBRTION OF NUMERICAL MODEL .....	4-4
4.5.	THE PARAMETRIC ANALYSIS .....	4-8
4.6.	BUCKLED WAVE FORM AMPLITUDE AND LENGTH.....	4-9
4.7.	CRITICAL OVALITY .....	4-12
4.8.	L/D DISCUSSION.....	4-19
4.9.	CONCLUSIONS.....	4-21
4.10.	REFERENCES .....	4-22
5.	THESIS CONCLUSIONS AND RECOMMENDATIONS.....	5-1
5.1.	CONCLUSIONS.....	5-1
5.2.	RECOMENDATIONS .....	5-2
6.	REFERENCES .....	6-1

### LIST OF FIGURES

Figure 2-1:	Critical Wavelength versus D/t (Ju and Kyriakides, 1992) .....	2-6
Figure 2-2:	Pipe Buckling Data Base (Zimmerman, 1995) .....	2-8

Figure 2-3: Pipe Buckling Data Base (Zimmerman, 2004) .....	2-8
Figure 2-4: DNV OS-F101 (2000) Girth Weld Factor Definition.....	2-14
Figure 2-5: Comparison of DNV (2000) and CSA (2003) Strain Limits .....	2-14
Figure 3-1: Finite Element Model and Physical Test Frame (Mohareb et al., 2001) .....	3-2
Figure 3-2: Second Order Moment Effects.....	3-2
Figure 3-3: Pressurized Outward Buckle.....	3-5
Figure 3-4: Unpressurized Inward Buckle.....	3-5
Figure 3-5: Finite Element Schematic .....	3-9
Figure 3-6: Calibration to Ghodsi et al. (1994).....	3-12
Figure 3-7: Calibration to Dorey (2001).....	3-12
Figure 3-8: Parametric Results – $D/t = 30$ .....	3-16
Figure 3-9: Parametric Results – $D/t = 60$ .....	3-17
Figure 3-10: Parametric Results – $D/t = 90$ .....	3-17
Figure 3-11: Trend for $D = 609.6\text{mm}$ , $N = 0.15$ .....	3-18
Figure 4-1: Finite Element Schematic .....	4-5
Figure 4-2: Calibration to Ghodsi et al. (1994) and Dorey (2001) .....	4-7
Figure 4-3: Measuring Variation from Global Curvature.....	4-10
Figure 4-4: Critical Ovality Measurement.....	4-12
Figure 4-5: Ovality Measurement for Diameter .....	4-14
Figure 4-6: Ovality Measurement for $D/t$ Ratio .....	4-15
Figure 4-7: Ovality Measurement for Pressure Ratio .....	4-16
Figure 4-8: Ovality Measurement for Axial Load Ratio .....	4-17

Figure 4-9: Ovality Measurement for Misalignment .....	4-18
Figure 4-10: Buckled Profile for $L/D = 3.5$ .....	4-19
Figure 4-11: Buckled Profile for $L/D = 5.5$ .....	4-20
Figure 4-12: Buckled Profile for $L/D = 10$ .....	4-20

### LIST OF ABBREVIATIONS AND SYMBOLS

$A_s$	Cross sectional Area of Steel
CSA	Canadian Standards Association
D	Pipeline Outside Diameter
D/t	Diameter to Thickness Ratio
$D_m$	Mean Pipeline Diameter
DNV	Det Norske Veritas
E	Elastic Modulus
$E_s$	Elastic Modulus of Steel
$F_{Axial}$	Applied Axial Force
$f_0$	Normalized Ovality
$F_y$	Force to Yield Pipe Section Axially
$h_{Offset}$	Measured Distance From End Cap to Reference Point
L	Pipe Length
L/D	Pipe Length to Diameter Ratio
LPF	Load Participation Factor
$M_{DNV}$	DNV (2000) Design Moment
MPC	Multi-Point Constraint

$M_{\text{end}}$	Applied End Moment
$N$	Normalized Applied Axial Force
$NPS$	Nominal Pipe Size
$P$	Applied Pressure
$p_b$	Burst Pressure
$p_c$	External Pressure
$p_i$	Internal Pressure
$p_{\text{min}}$	Minimum Internal Pressure
$P_y$	Pressure to Yield Pipe Section Circumferentially
$t$	Pipeline Wall Thickness
$t_n$	Nominal Wall Thickness
$\Delta T$	Change in Temperature
$\alpha$	Coefficient of Thermal Expansion
$\alpha_{\text{gw}}$	Girth Weld Factor
$\alpha_h$	Maximum Allowed Yield to Tensile Strength Ratio
$\beta$	Pressure Stress Ratio
$\Delta\theta_{\text{Ends}}$	Differential End Rotation
$\delta R$	Variation From Global Curvature
$\epsilon_c$	Compressive Strain Limit
$\epsilon_c^{\text{crit}}$	Critical Compressive Strain
$\epsilon_{\text{DNV}}$	DNV (2000) Characteristic Strain

$\kappa$	Global Curvature
$\nu$	Poisson Ratio
$\theta$	Rotation Measured at Reference Point
$\sigma_a$	Axial Stress
$\sigma_h$	Circumferential (Hoop) Stress
$\sigma_y$	Yield Stress

### **LIST OF APPENDICES**

Appendix A: Tabulated Results of Parametric Study .....	A-1
---	-----

# **1. INTRODUCTION, OVERVIEW AND CO-AUTHORSHIP STATEMENT**

## **1.1. INTRODUCTION**

The ever expanding oil and gas industry is constantly pushing the boundaries of what are feasible and economical energy development projects. With exploration in deep water and harsh environmental conditions, especially in the Arctic, new technical challenges arise when transporting resources via pipeline. One of these challenges is to design against pipeline buckling on both local and global scales.

Many researchers have studied buckling of pipelines under combined loading, or loading from axial, bending and pressure, as it arises in many of the challenging field developments. In the Arctic, for example, pipeline designs have to account for potential permafrost heave, thaw settlement and/or ice gouging if the pipeline is installed in offshore regions. In deep water applications, excessive bending from installation and external pressure impose a substantial risk to the mechanical integrity of the pipeline. In both these scenarios, any given loading combination may trigger local or global buckling rendering the pipeline unserviceable, or worse, result in catastrophic failure and hydrocarbon release.

## **1.2. OVERVIEW**

The objective of this research is to investigate the effects of girth welded pipe on buckling capacity for moment and strain. By studying published works on the buckling behaviour of pipelines, a greater understanding of the subject was obtained. The

literature review presented here describes physical, analytical and numerical methods that have been used to characterized buckling behaviour. Based on this review, a numerical procedure using finite element methods was developed to model the buckling and post-buckling response of pipeline subject to combined stress state.

While the literature review contains a large collection of data based on a wide range of parameters, few of these studies present all of the information required to properly calibrate a numerical model. The research program conducted at the University of Alberta provides the most comprehensive public domain dataset available. Selected studies from this research program were used in the calibration of the numerical procedures in this thesis.

After calibrating the numerical model and procedures to physical test data, a parametric study was developed to investigate moment and strain capacity, pipeline ovality and buckle wave forms and amplitude based on five design parameters. These included; pipeline diameter, wall thickness, applied internal pressure, applied axial force and girth weld misalignment amplitude.

### **1.3.CO-AUTHORSHIP STATEMENT**

This research topic was proposed to the principal author by Dr. Shawn Kenny, Memorial University of Newfoundland. His contribution to this body of work was to direct the author in areas of interest pertaining to buckling capacity of pipelines. Dr. Shawn Kenny

and Dr. Ryan Phillips, C-CORE, have both played a role in the review of this manuscript and published works, as well as provided comments on the revision of these documents.

The principal author was responsible for composing this thesis, conducting literature review, data synthesis and analysis, conducting the parametric study, interpreting results and developing conclusions and recommendations from this study.

## **2. LITERATURE REVIEW**

### **2.1. EXPERIMENTAL AND ANALYTICAL INVESTIGATIONS**

Early studies on the behaviour of pipelines generally involved experimental and analytical methods. Jirsa et al. (1972) performed physical testing on concrete coated steel pipes ranging in diameter from 10.75 to 20 inches, to investigate the influence of ovaling on flexural behaviour when tested under four-point bending. Moment-Curvature relations were determined by inferring the applied moment and curvatures from finite difference expressions of the applied loads and strain measurements, respectively.

The experimental results of Jirsa et al. (1972) were compared to analytical results derived from the principle of least work presented in Wilhoit et al. (1971), established by Ades (1957), concluding ovalization does not significantly reduce the moment capacity of pipes and the concrete coating has little effect on the ovaling characteristics.

Bouwkamp et al. (1973) developed an experimental test program using a vertical four-point bending test, similar to that of Jirsa (1972), with the addition of an applied axial load. The motivation for this experiment was to establish deformation criteria for the Trans-Alaskan pipeline system considering 48 inch diameter, X60, pipe under combined loading conditions. Seven pipe segments were tested with respect to various internal pressures and temperatures while accounting for end effects by way of applying equivalent axial forces. Buckling occurred in two distinct patterns; outward bulging in

the pressurized cases and diamond-shaped inward-outward deformation in the low pressure cases.

Johns et al. (1975) and Johns et al. (1977) took an experimental and analytical approach to investigate the buckling of cylindrical columns. The physical experimentation of 1.25 and 2 inch diameter pipelines,  $D/t$  ratio of 60, was tested using four-point bending inside a containment chamber that allowed for external pressure. The analytical procedure was based on thin shell theory and the complex analytical expressions were solved by the process of enumeration, methodical trial and error, to find the lowest possible wave number of buckling.

Reddy (1979) investigated small diameter pipelines as well, testing a total of 19 pipe samples, 10 steel and 9 aluminum. The pipelines were one inch in diameter, 24 inches in length and had  $D/t$  ratios ranging from 30 to 80. Reddy (1979) used results from Bouwkamp et al. (1973), as well as Wilnoit et al. (1973), and the theoretical predictions of Batterman (1965), to assess critical compressive strains obtained from experimental tests on both steel and aluminum alloys pipelines. Reddy (1979) concluded that wave type ripples trigger collapse rather than small amounts of ovalization.

Kim (1992) aimed to simplify analytical equations, based on  $J_2$  deformation theory and energy methods similar to the works of Batterman (1965), used for axisymmetric bifurcation analysis by investigating both experimental and theoretical results for

pipelines under combined loading. Kim (1992) indicated that the primary factors dominating buckling failure are: i) initial imperfection; ii) diameter to thickness ratio; iii) pipe end conditions and length; and iv) internal pressure. Kim (1992) emphasizes that critical strain under combined loading can be considerably greater than critical strain under pure bending alone. In particular, internal pressure effects have been shown to be beneficial, providing a margin of safety for pipelines designed on the basis of zero internal pressure.

Using cantilever and fixed ended beams, the experimental work of Sherman (1976) on steel tubes, 270mm in diameter and  $D/t$  ratios ranging from 18-102, consisted of two series of tests which primarily studied the effect of shear through the pipe section. Sherman (1976) made several conclusions regarding strength, critical strains and post-buckling behaviour. The strength of the section is greatly affected by the presence of shear for sections with  $D/t$  ratios greater than 55 due to the inadequacy of the sections to redistribute moments. Small moment gradients in the cantilever tests resulted in higher strains measured at the initial buckle when compare to constant moment tests. Post-buckling behaviour is related to  $D/t$  ratio and a function of yield strength.

## **2.2. NUMERICAL AND PARAMETRIC INVESTIGATIONS**

Numerical buckling analysis of pipelines is used predominantly in recent literature which was initiated by the development and availability of computers. Physical experimentation is still required, however, to obtain confidence in results obtained by numerical simulation. Numerical procedures are very cost effective in that many

parameters can be studied at minimal cost in order to extend the range of physical testing program.

Kyriakides and Ju (1992) conducted a series of physical tests on aluminum tubing to study the effect of bending on long cylindrical shells, which was then used to develop a numerical procedure to predict the deformation behaviour, Ju and Kyriakides (1992). As referenced in Kyriakides and Ju (1992), the natural limit load of cylindrical shells is characterized by the "Brazier Effect" (Brazier, 1927), whereby circular tubes under bending will tend to ovalize. The growth of this ovalization results in a natural reduction in the bending strength on the shell, due to reduced rigidity, until a maximum bending moment is achieved.

As shown by experimentation, in addition to limit load instabilities as a result of both ovalization and plastic material properties, shell bending is also limited by shell buckling modes. As shell structures are bent, short wavelength ripples were observed experimentally on the compression side of the shell tubing, which in turn triggered the localization of ovalization. As the natural limit load is approached, the long wavelength imperfections become amplified resulting in non-uniform ovalization. As previously mentioned, the development of ripples and waveform imperfections has been documented in Reddy (1979) as well.

The experiments of Kyriakides and Ju (1992) on aluminum tubing studied  $D/t$  ratios from 19.5 to 60.5. The authors describe a change in buckling behaviour as  $D/t$  decreases. For  $D/t > 40$ , the prevalent mode of instability was short wavelength rippling, characteristic of shell mode type buckling, which occurred in small regions randomly distributed over the length of the test section. The shells were found to ovalize relatively uniformly until collapse, which were generally diamond-shaped for zero pressure, typical of elastic shell buckling. Since bending strains at the initiation of rippling were much lower than the corresponding strain at limit load, it was stated that the two instabilities showed no signs of interaction.

For intermediate  $D/t$  tests, ranging from 26 to 40, short wavelength rippling was evident. A limiting moment was clearly defined in these tests, unlike tests for  $D/t > 40$ . Evidence from these tests indicate that the natural limit load and rippling instability begin to interact as the curvature at which rippling occurs becomes closer to the limit load induced by ovalization.

For the thick walled pipes,  $D/t < 26$ , longer wavelength imperfections govern the shells bending capacity as the pipe approaches that of a beam bending. Ovalization becomes much more non-uniform and localizes significantly following the limit load. With the limit load instability dominating the failure mode, the natural load limit calculated by considering Brazier Effect is representative of the actual value.

The key result of the Kyriakides and Ju (1992) study concludes that the local buckling response varies significantly over the range of D/t. For D/t ratios in the 20-40 range, of practical importance for arctic ice gouge and deepwater applications, the primary mode of buckling is due to ovalization. For D/t ratios greater than 40, typical for onshore pipelines, the buckled mode is triggered by the formation of ripples. The effect of D/t on buckling wavelength, presented in Ju and Kyriakides (1992), is shown in Figure 2-1.

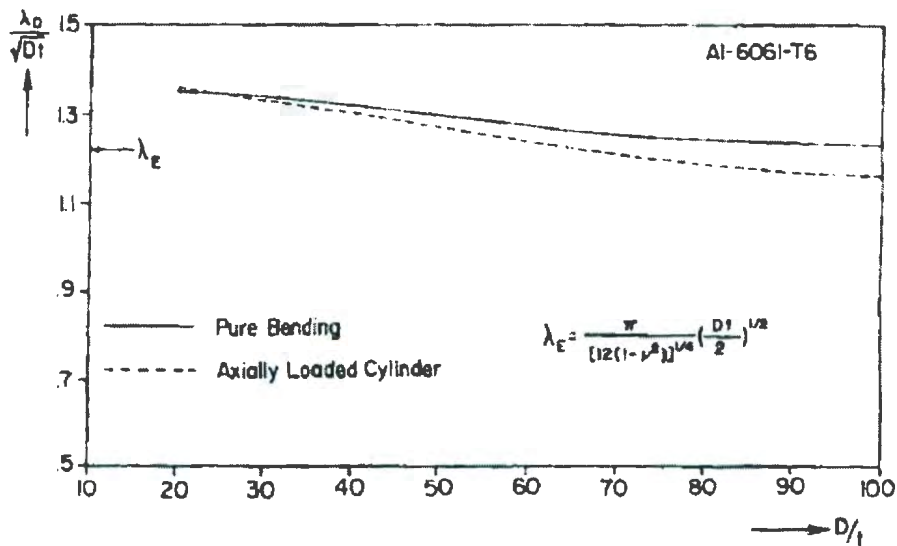


**Figure 2-1: Critical Wavelength versus D/t (Ju and Kyriakides, 1992)**

Further to the experimental work of Kyriakides and Ju (1992), Ju and Kyriakides (1992) developed analytical expressions and numerical procedures to capture the complex nature of cylindrical shell buckling. Sanders' shell kinematics and the principal of virtual work were used as basis for a numerical model capable of: 1) modeling ovalization at the cross-section of the hollow cylinder, 2) simulating the growth of short wavelength axial ripples, and 3) allow for the shell to localize and long wavelength amplitudes over a few diameters.

The results of the numerical procedures were largely successful in capturing the behaviour of the cylindrical shells as compared to experiments; however, there was a discrepancy noted between the critical wavelengths calculated and those recorded during physical testing. This discrepancy was later attributed to anisotropy (Kyriakides and Corona, 2007). The critical curvature yielded by the analysis was in good agreement with the physical tests.

Using a finite element method, Row et al. (1983) studied the influence of material properties, imperfection type and size, and applied pressure and forces on pipeline buckling, which, as indicated in both the presented thesis and Row et al. (1983) report, proved to be significant design factors. These analyses were correlated against the large scale tests of Bouwkamp et al. (1974).

Imperfections were idealized using both bulge and offset eccentricities, the later showing a greater significance on critical buckling strain. It was shown that the compressive strain limit decreases with increasing amplitude and decreasing wavelength of the imperfection and the effect of imperfection is more sensitive at low pressure. Row et al. (1983) studied the potential for depressurization to trigger wrinkle formation as critical strain limits decrease with decreasing pressure. However, Row et al. (1983) also shows numerically that when a pipeline is depressurized at constant axial strain the pipeline does not wrinkle.

Zimmerman et al. (1995) provided a comprehensive assessment of compressive strain limits for buried pipelines including the most predominant methods of analysis and criteria at the time. The report discussed methods of analytical and experimental analysis in published works and provided a thorough summary of the experimental data available as well as established empirical equations. This information is given in Figure 2-2 which was later updated in Zimmerman et al. (2004) shown in Figure 2-3:

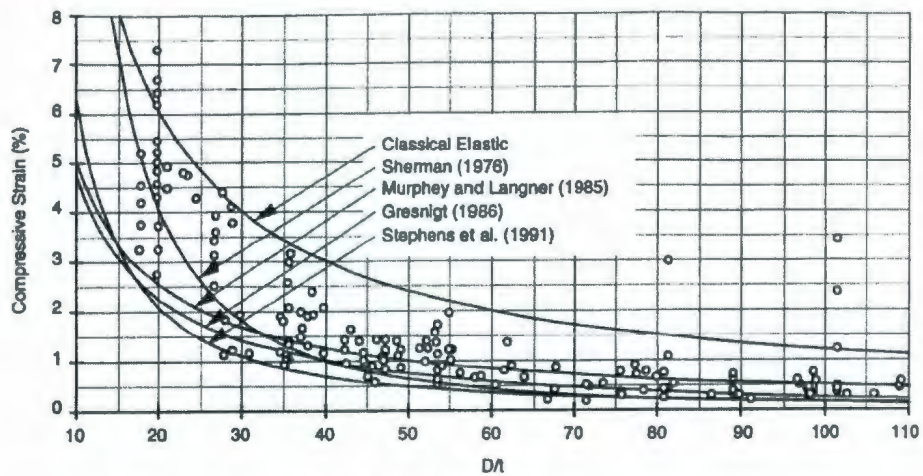


Figure 2-2: Pipe Buckling Data Base (Zimmerman, 1995)

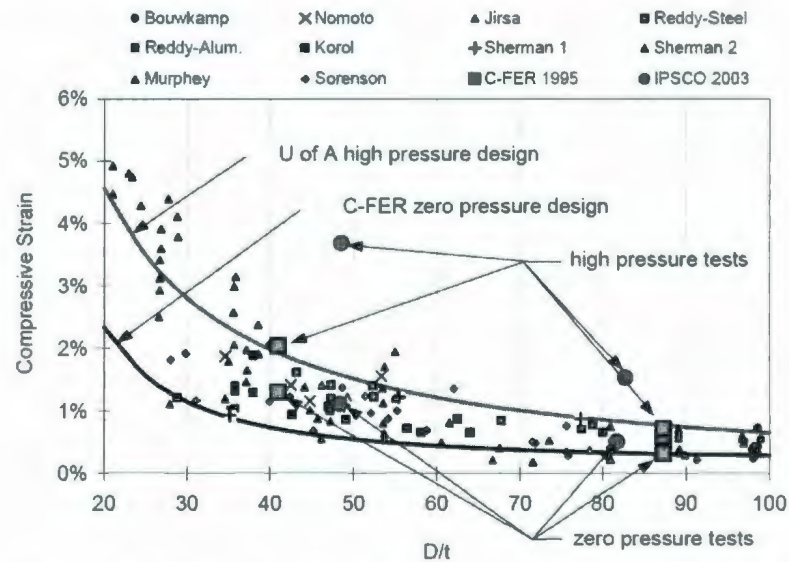


Figure 2-3: Pipe Buckling Data Base (Zimmerman, 2004)

In addition to analytical methods and physical testing approaches, Zimmerman et al. (1995) discussed the development of finite element analysis for strain based design. Models were calibrated to large-scale combined loading tests done at C-FER, the Centre for Frontier Engineering Research. This work then provided the foundation to pursue a numerical parametric study investigating the  $D/t$  ratio, internal pressure, material yield strength, variations in the material stress-strain curve and degree of applied axial tension.

Several conclusions were drawn from the finite element analysis. It was found that i) decreasing the  $D/t$  ratio increased peak moment and strain, ii) increasing internal pressure decreased peak moment but increased peak strain, iii) an increased plastic modulus results in both increased peak moment and strain, and iv) axial tension delayed yielding, increased peak moment and increased peak moment curvature.

The notion of developing a “numerical testing laboratory” using finite element methods in order to study pipeline buckling behaviour is presented by Bruschi et al. (1995). By developing numerical procedures, the overall cost and time required for the test program is reduced because only a select number of physical tests are needed to calibrate the numerical model.

Once Bruschi et al. (1995) had a calibrated model against Reddy (1979) and Mohareb et al. (1993), the authors used response surface methodology to formulate regression equations based on numerical results. Six responses were monitored (moment, curvature

and axial strain measured at both the limit point and onset of buckling) as result of two input parameters (pressure and applied axial load), whereas element type, mesh density and material property definitions were held constant.

Vitali et al. (1999), building on Bruschi et al. (1995), extended the developed numerical procedures to investigate the influence of pipe diameter to thickness ratio, material properties and axial load as well as internal pressure for a total of 120 simulations.

The findings of the parametric study in Vitali et al. (1999) confirmed that:

- Pressurized pipelines typically buckle in an outward bulging manner whereas unpressurized pipelines develop inward diamond or inward/outward diamond shaped buckling modes depending on the diameter to thickness ratio.
- Peak bending moment capacity decreases as the hardening of the pipe material decreases, axial force ratio decreases (increasing compression), and diameter to thickness ratio increases.
- Minimum compressive strains, i.e. strains measure at maximum moment, increase with increased internal pressure as well as increased hardening of the pipe material.

Furthering the numerical research, Torselletti et al. (2005) focused on the effects of girth or circumferential welds on maximum bending moments and corresponding compressive strain limits. Using the finite element model developed in Vitali et al. (1999), a

parametric study was done with the intent of comparing bending capacity and critical strain limits predicted using finite element methods with the DNV OS-F101 (2000) design equations. Offset misalignment and ovality were introduced as girth weld imperfections in the model. Ovality imperfection was shown to have less of an effect, as compared to translational offset, on reducing moment capacity and critical strain limit. The sensitivity to misalignment becomes less prevalent for lower  $D/t$  ratios.

Dorey et al. (2006) emphasized the importance of modeling initial imperfection in order to achieve good correspondence to physical experimentation. Prior to the physical experiment referenced in Dorey et al. (2006), a series of dimensional measurements were taken to more accurately capture the initial geometry of the test section. In mapping the imperfection grid to the mesh of the finite element analysis, the authors have shown very good correspondence to the physical experiment for both welded and plain pipes.

Since measuring each pipe segment is impractical and expensive, Dorey et al. (2006) idealizes imperfections for plain and girth-welded pipe by using half sine wave and offset imperfections, respectively. Using these single imperfections at the mid-section of the numerical analyses, the authors were able to characterize the buckling behaviour of the test sections measured in detail.

Consistent with Dorey et al. (2006), Fatemi et al. (2006) conducted a finite element parametric study using parameters D/t ratio, internal pressure, axial load, and geometric imperfections to study the effects of local buckling of a pipeline under combined loading. The study investigated perfect or ideal pipeline geometry as well as imperfect pipeline geometry with single blister-type imperfections. For a D/t ratio of 70, three different buckling modes were shown over varying pressure stress ratios ( $\beta$ ); for  $\beta < 0.15$  an inward buckle, for  $0.15 < \beta < 0.35$  a single outward buckle and for  $\beta > 0.35$  an outward double buckle characteristic of a higher mode buckled shape. Axial load effects were also investigated over a range of D/t values at a constant internal pressure to stress ratio of 0.8.

### 2.3. PIPELINE DESIGN CODES AND GUIDELINES

Design codes and guidelines are written to protect the general public and given minimum requirements for pipeline design using simplistic equations. The Canadian Standards Association design code for oil and gas pipelines is dictated by CSA Z662 (2003). Contained within Annex C of the code for limits states design, a strain equation developed by Gresnigt (1986) for the longitudinal compressive strain limit for buckling is given as follows:

$$\varepsilon_c^{crit} = 0.5 \frac{t}{D} - 0.0025 + 3000 \left( \frac{(p_i - p_e)D}{2tE_s} \right)^2 \quad (2-1)$$

where,  $E_s$  is the elastic modulus for steel (207 GPa) and  $p_i$  and  $p_e$  are internal and external pressures, respectively.

As one can see from the equation, no allowance is given for the effects of girth welding or other imperfections which is believed to be a significant omission based on the literature review conducted, although the code limits the girth weld offset to a maximum of 1.6 mm.

Design code DNV OS-F101, Submarine Pipeline Systems, incorporates limit-state design with calibrated safety factors to stipulate recommended strain limits for pipelines under combined loading while including some allowance for girth weld imperfection. The strain equation is intended for use in an offshore installation setting. The characteristic strain equation is given as (DNV OS-F101, 2000):

$$\epsilon_c = 0.78 \left( \frac{t}{D} - 0.01 \right) \left( 1 + 5 \frac{\sigma_h}{f_y} \right) \alpha_h^{-1.5} \alpha_{gw} \quad (2-2)$$

where  $\sigma_h$  and  $f_y$  are hoop stress ( $\Delta P(D-t)/2t$ ) and yield stress, respectively. Design factors  $\alpha_h$  and  $\alpha_{gw}$  are included to account for material hardening and girth weld effects.

The girth weld factor is simplistically defined as a bilinear curve, shown in Figure 2-4. “The reduction is expected to negligible at  $D/t = 20$ . A linear interpolation is then proposed up to  $D/t = 60$ ” (DNV OS-F101, 2000) where a reduction in compressive strain capacity was found to be on the order of 40% based on the works of Ghodsi et al. (1994) to yield a girth weld factor of 0.6.

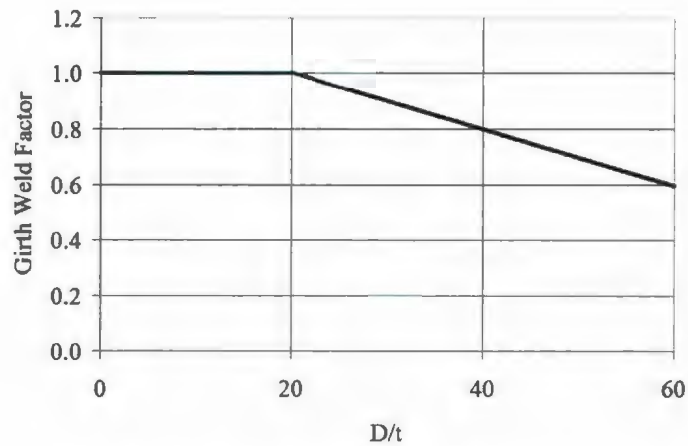


**Figure 2-4: DNV OS-F101 (2000) Girth Weld Factor Definition**

A comparison of CSA and DNV design equations are shown in Figure 2-5 for a pipeline, having yield strength of 448MPa (X65), at zero and 80% design pressure. The DNV characteristic strain equation is factored using a resistance strain factor of 2.6 to yield a design strain.

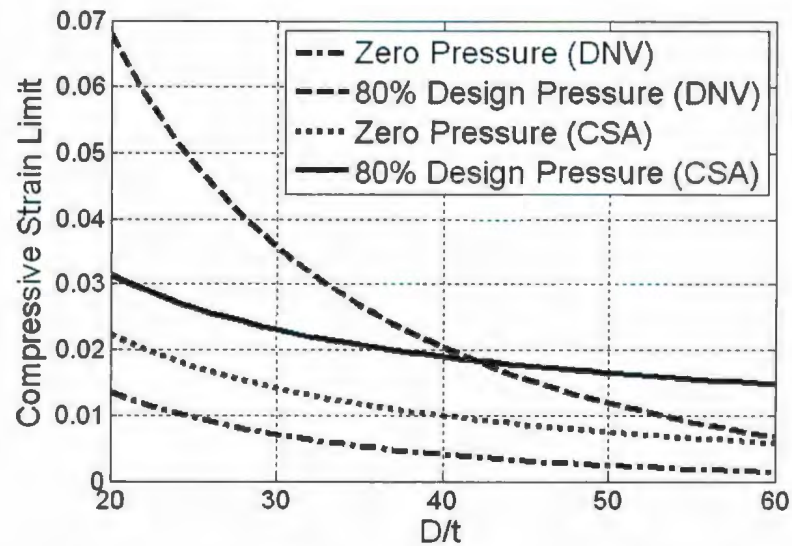


**Figure 2-5: Comparison of DNV (2000) and CSA (2003) Strain Limits**

It should be noted that the DNV critical strain equation was developed for offshore use where pipeline are generally thicker than onshore pipelines. Thus the equation is only valid for  $D/t$  ratios less than 45. Regardless, a large difference between the CSA and DNV strain capacity equations is shown between design equations within the  $D/t$  range of 20 to 45.

#### **2.4. SUMMARY**

A review of pipeline buckling experiments, both analytical and numerical analysis methods, and pipeline design codes has been presented. Many physical experiments have been documented characterizing pipeline buckling by studying many pipeline design parameters. The scatter of critical strain data, seen in Figure 2-2 and Figure 2-3, can be attributed to variations in pipeline geometry, material properties and loading conditions. Various buckling mode shapes and responses have been shown to vary from thick-walled to thin-walled pipeline and they also show strong dependencies on applied pressure. As the focus of the present research is on girth welding effects in steel pipelines, studies of geometric imperfection in welded pipelines are of greater interest.

### **3. OMAE 2009 – EFFECTS OF GIRTH WELD ON THE LOCAL BUCKLING RESPONSE OF CONVENTIONAL GRADE PIPELINES**

*Submitted to: 28th International Conference on Ocean, Offshore and Arctic  
Engineering*

*Authors: John Barrett, Shawn Kenny and Ryan Phillips*

*Reviewed and Accepted on: February 7, 2009*

#### **3.1. SYNOPSIS**

The most detailed account of physical experiments involving girth welded pipelines were produced at the University of Alberta through the works of Ghodsi et al. (1994) and Dorey (2001) and are used as the foundation of the research presented in this thesis. In the following OMAE 2009 paper, a numerical finite element modelling procedure was developed to assess the bending moment and strain capacity of girth welded pipelines over typical design parameters. A finite element method of analysis was adopted for this research due to lack of direct access to physical testing facilities. Figure 3-1 illustrates the finite element model used in the analysis as well as a schematic of the U of A testing apparatus.

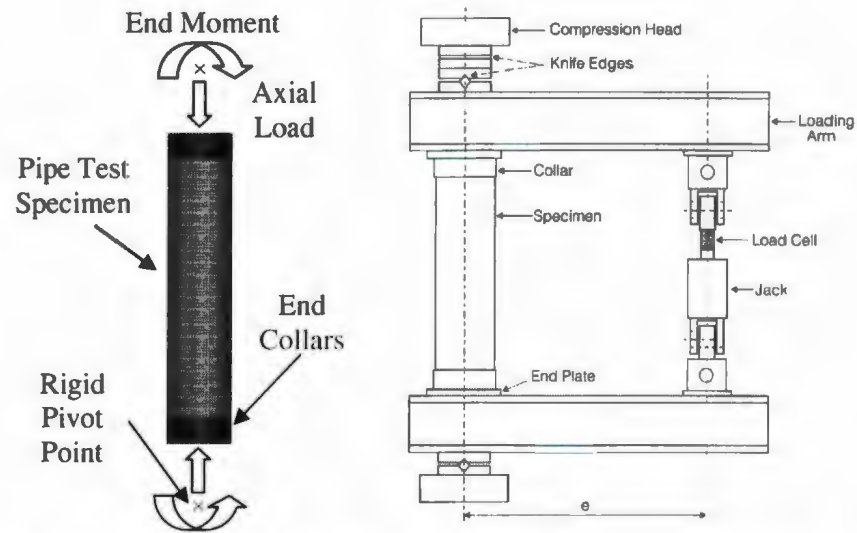


**Figure 3-1: Finite Element Model and Physical Test Frame (Mohareb et al., 2001)**

As in the physical experiment, secondary end moment effects are generated due to the applied axial force acting on the pivot point / knife edge, indicated in Figure 3-1, in addition to the applied end moments generated by the load cell and loading arm. These secondary effects are significant, as illustrated in Figure 3-2, when considering the global buckling response of the system as end rotation (curvature) increases.

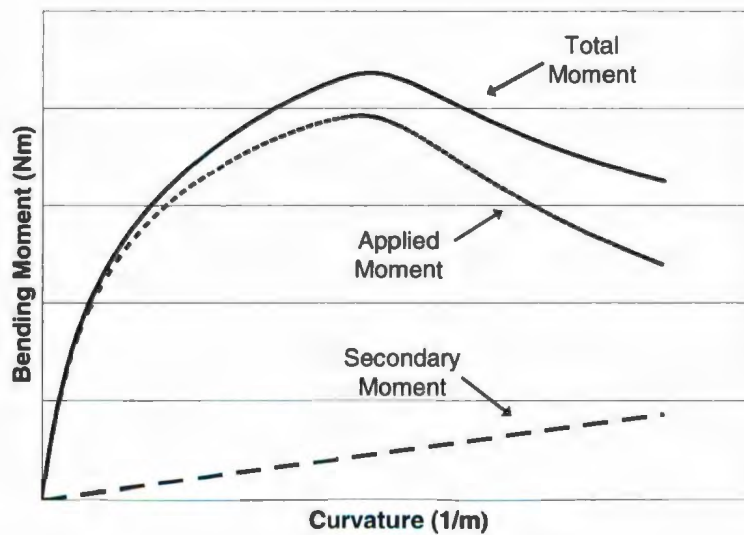


**Figure 3-2: Second Order Moment Effects**

In this study, the pipelines were modeled using reduced integration shell elements (ABAQUS shell element S4R). As stated in the following OMAE 2009 paper, the element mesh density for the calibration analysis was selected to be consistent with Al-Showaiter et al. (2008) for the physical test of Ghodsi et al. (1994) and based on Dorey's own numerical analysis in Dorey (2001). The calibration analysis was shown to be consistent with both sets of physical data using these mesh densities and therefore an extensive mesh sensitivity study was not carried out. It is acknowledged, however, that mesh density can have a dramatic effect on buckling response of the analysis. The amplitude of the misalignment imperfection was varied in the calibration analysis to obtain correspondence to the physical data given by Ghodsi et al. (1994) and Dorey (2001).

Based on the literature review, five design factors were chosen to parametrically investigate the local buckling behaviour. These factors included: diameter, diameter to thickness ratio, pressure-stress ratio, axial load ratio and initial imperfection amplitude. Due to limited material property data, material effects were not investigated. Therefore, the scope of the investigation was limited to these five factors. The Ramberg-Osgood formulation, as defined in Walker and Williams (1995), was used to define the material property, having specified yield strength of 483 MPa (X70), in the parametric analysis.

As in Torselletti et al. (2005), the DNV (2000) compressive strain equation was used to compare the 243 results of the parametric analysis despite the fact that the strain equation

is only applicable for  $D/t$  ratios less than 45. The results of the parametric analysis presented graphically in the OMAE 2009 paper are reproduced in tabular form in Appendix A. The results for pure bending are shown to be consistent with that presented in Torselletti et al. (2005). However, including an applied axial load and pressure effects in combination has shown to greatly reduce the strain and moment capacity of the pipeline.

The OMAE 2009 paper concludes that an increased axial force decreases critical moment as well as critical strain by as much as 40% and 50% for both moment and strain, respectively. The maximum degree of imperfection, 15% of wall thickness, is shown to reduce the moment and strain capacities by about 10% and 35% for moment and strain, respectively.

The strain behaviour, with respect to pressure, is shown to be non-linear. This is due to the different buckling modes triggered; outward bulge for pressurized cases (Figure 3-3) and inward diamond buckles for low pressure cases (Figure 3-4). It is recommended that the design strain criteria be dependant on the buckling mode of the pipe as the failure mode changes from pressurized to unpressurized pipes.



**Figure 3-3: Pressurized Outward Buckle**



**Figure 3-4: Unpressurized Inward Buckle**

### **3.2. ABSTRACT**

Pipeline structural integrity is a critical component of pipeline design for extreme environmental conditions. Severe loads may be an issue in pipeline design if differential ground movement is prevalent in the design region, e.g. ground faulting or permafrost heave / settlement. Iceberg or ice keel interaction and large seabed deformations interacting with the pipeline may also be a critical design integrity issue for offshore pipelines in ice environments.

Numerical finite element modelling procedures have been developed to assess the bending moment and strain capacity of several pipelines over a range of typical pipeline parameters. This study looks at the effects of girth-weld imperfection on the bending response of welded pipelines. Limited guidance is provided by pipeline design standards,

for example DNV OS-F101 and CSA Z662, as to how to account for girth weld effects on the local buckling response. This paper investigates girth weld effects across a range of practical design parameters.

Calibration of the numerical analysis was performed using available data, from full-scale tests and finite element analysis, for girth welded pipes in order to obtain confidence in the numerical procedure. The significance of girth weld effects was to reduce the peak bending moment capacity by 10% whereas strain capacity was reduced by as much as 35% based on the degree of girth weld imperfection. Girth weld effects have been acknowledged in industry; however, further research and physical testing is required to fully understand the problem, as shown in this paper.

### **3.3. INTRODUCTION**

The demand for oil compels developers to venture into new and more challenging environments where design loads on pipelines may be uncertain. Some of the most difficult design conditions are found in the Arctic where many forms of extreme loading conditions influence the design of pipelines; for example ground movement induced permafrost heave / settlement, as well as subgouge deformations due to the interaction of ice features with the seabed. Iceberg loading events are also of concern for pipelines and offshore installations on Canada's east coast.

Physical testing of full scale pipelines is often difficult, time consuming and generally expensive. It may be difficult to capture all loading conditions in a single test program.

Numerical finite element analysis is therefore a beneficial tool in design of pipeline systems that can readily supplement physical test programs. Once properly developed, the numerical tools can rapidly and efficiently simulate many various loading conditions that cannot be done economically in a physical laboratory setting. This paper discusses the development and calibration of a numerical model for girth welded pipelines under combined loading conditions, demonstrates its applicability over a range of pipeline design parameters, then explores the significance of the girth welded imperfection parametrically.

#### **3.4. CALIBRATION OF NUMERICAL MODEL**

The commercial finite element package ABAQUS v6.7 was used to develop a buckling analysis based on the works of Ghodsi et al. (1994) and Dorey (2001). Ghodsi et al. (1994) undertook a physical test program and considered 12 test cases at three different pressure levels for two different diameters. The selected 304.8mm (12 inch) and 508mm (20 inch) outer diameter pipes were fabricated using the UOE process, a common fabrication process in pipeline construction where steel plates are bent into a U-shape, then into an O-shape and then Expanded to form a circular section. The 304.8mm (12 inch) and 508mm were of pipe grades of X52 and X56, respectively. The authors' nomenclature for the experimental program, XYZnn(W), is summarized as follows:

- X = U, D, or H representing Upstream (unpressurized), Downstream (fully pressurized to 72% or 80%) and Halfway (pressurized to 36% or 40%)
- Y = G or L representing Greatest and Least thermal effect
- Z = A or R representing Active or Reactive axial force end conditions.

$n_n$  = Nominal diameter (in inches)

W = Indicating that the pipe is Welded at mid-span

Dorey (2001) conducted a series of physical experiments as well as numerical analyses and compared the results to a large catalogue of data including the works of Ghodsi et al. (1994) and Mohareb et al. (1994). Dorey's physical tests consisted of NPS 30 pipe sections with an outside diameter of 762 mm with a thickness of 8.3 mm with specified yield strength of grade X70. Dorey's tests conducted under initial compression are of interest to this calibration study. These tests were denoted as CP##W, where ## represents 0, 20, 40 and 80% of the pressure to cause yield in the circumferential direction of the pipe section, or pressure-stress ratio  $\beta$ , which is given in equation (3-1).

$$\beta = \sigma_h / \sigma_y = (PD_m / 2t_n) / \sigma_y \quad (3-1)$$

The physical test procedure for both experiments stipulated that the pipe was first pressurized to the required level. An axial force was also applied to compensate for thermal loads, inferred from field conditions, axial Poisson effect deflections and end cap effects, which are not present in continuous pipelines in the field. The total applied axial force is resolved by summing the following forces for thermal, Poisson, and end cap effects, equations (3-2) through (3-4), respectively.

$$F_t = \alpha A_s E \Delta T \quad (3-2)$$

$$F_v = -\nu A_s (PD_m / 2t_n) \quad (3-3)$$

$$F_p = (\pi/4 D_m^2)P \quad (3-4)$$

A multi-point constraint (MPC) was used to model the end boundary conditions for the pipe test segment. This allowed for the circumferential nodes at the end of the pipe to be tied to one single reference node, located at a specified pivot point. This constraint allows for control of the end section as a whole permitting only bending rotation and axial translation at the ‘free end’ where the applied axial load is applied. The MPC used in this analysis does not, however, allow for the end section to ovalize. This is not believed to be a substantial error since the experimental pipe test section was connected to the test frame via an end plate where the circumferential support collars were used to reduce stress concentrations near the endplate. An illustration of the developed finite element model is given in Figure 3-5.

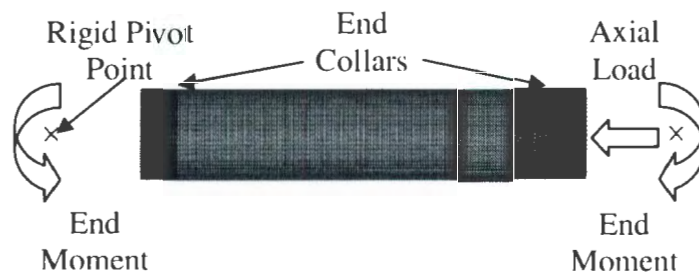


**Figure 3-5: Finite Element Schematic**

Using the Modified Riks method, for nonlinear solution, concentrated end moments were applied to the end reference pivot points. The ABAQUS load participation factor (LPF) was used to calculate the applied end moments. Second order effects arising from the applied axial force were also accounted for, modified slightly from Mohereb et al. (2001), using the following equation,

$$M_{\text{End}} = M_{\text{LPF}} + Fh_{\text{Offset}} \text{Sin}(\theta) \quad (3-5)$$

where  $h_{\text{Offset}}$  is the distance from the end cap to the rigid reference point and  $\theta$  is measured from the reference point of the applied axial load. Global curvatures were calculated based on the differential rotation measured at the reference points over the pipe sections total length, as indicated by equation (3-6).

$$\kappa = \Delta\theta_{\text{Ends}} / L \quad (3-6)$$

A 4-noded shell element, with reduced integration and hourglass control (ABAQUS element S4R), was used as its formulation allows for large displacement and finite membrane strain. The circumferential to longitudinal mesh densities used in the calibration analysis of 324mm and 508mm pipes were 60 to 161, consistent with density used in Al-Showaiter et al. (2008). The mesh density used for the 762mm pipe was 40 to 75, as used in Dorey (2001). Two end collars that were used in the physical experiment to connect the pipe test section to the frame were also modelled numerically. All collars were 150mm in length and had the same thickness as the pipe section being analyzed. A summary table of the calibration analyses parameters for Ghodsi et al. (1994) is given in Table 3-1. The calibration analyses parameters for Dorey (2001) is given in Table 3-2. Table 3-3 contains the true stress-strain material data used for the calibration.

	UGA12W	HGA12W	DGA12W	UGA20W	HGA20W	DGA20W
D (mm)	324	324	324	508	508	508
$t_n$ (mm)	6.35	6.35	6.35	7.9	7.9	7.9
$D/t_n$	51	51	51	64	64	64
L (m)	1.69	1.69	1.69	1.69	1.69	1.69
$\beta$	0.00	0.36	0.72	0.00	0.40	0.80
P (MPa)	0.00	5.26	10.52	0.00	4.96	9.91
Grade	X52	X52	X52	X56	X56	X56
$h_{\text{Offset}}$ (mm)	162	162	162	254	254	254
F (kN)	667	822	978	1333	1701	2069

**Table 3-1: Ghodsi et al. (1994) Input Parameters for Calibration Study**

	CP00W	CP20W	CP40W	CP80W
D (mm)	762	762	762	762
t <sub>n</sub> (mm)	8.3	8.3	8.3	8.3
D/ t <sub>n</sub>	92	92	92	92
L (m)	2.7	2.7	2.7	2.7
β	0.00	0.20	0.40	0.80
P (MPa)	0.00	2.15	4.30	8.61
Grade	X70	X70	X70	X70
h <sub>off</sub> (mm)	381	381	381	381
F (kN)	2069	2437	2806	3548

**Table 3-2: Dorey (2001) Input Parameters for Calibration Study**

X52		X56		X70	
<u>Stress (Pa)</u>	<u>Strain (-)</u>	<u>Stress (Pa)</u>	<u>Strain (-)</u>	<u>Stress (Pa)</u>	<u>Strain (-)</u>
0.00E+00	0.00000	0.00E+00	0.00000	0.00E+00	0.00000
2.00E+08	0.00100	2.00E+08	0.00100	5.68E+08	0.00279
3.29E+08	0.00194	3.31E+08	0.00192	5.77E+08	0.01065
3.75E+08	0.00241	3.75E+08	0.00238	5.88E+08	0.02073
3.92E+08	0.00476	3.87E+08	0.00376	6.01E+08	0.03339
4.05E+08	0.01041	3.94E+08	0.00468	6.12E+08	0.04772
4.16E+08	0.02029	4.05E+08	0.01020	6.23E+08	0.06473
4.35E+08	0.03959	4.18E+08	0.02031	6.32E+08	0.08125
4.49E+08	0.05794	4.34E+08	0.03962	6.37E+08	0.10290
4.64E+08	0.07677	4.49E+08	0.05847		
5.21E+08	0.18218	4.62E+08	0.07732		
		5.19E+08	0.18261		

**Table 3-3: Calibration True Stress-Strain Definition**

The interests of Ghodsi et al. (1994) physical tests were in the strain measured at the initiation of the pipe wrinkling and buckling. Dorey (2001) established critical strain equations based on the numerical and physical results. These reports provided a basis to study the effects of girth welded pipelines more specifically. The results of OMAE 2009 calibration study, indicated by the solid data points, for Ghodsi et al. (1994) and Dorey (2001) are given in Figure 3-6 and Figure 3-7, respectively.

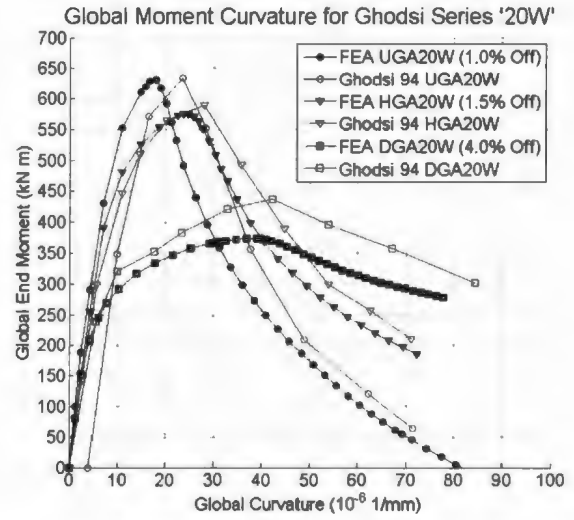
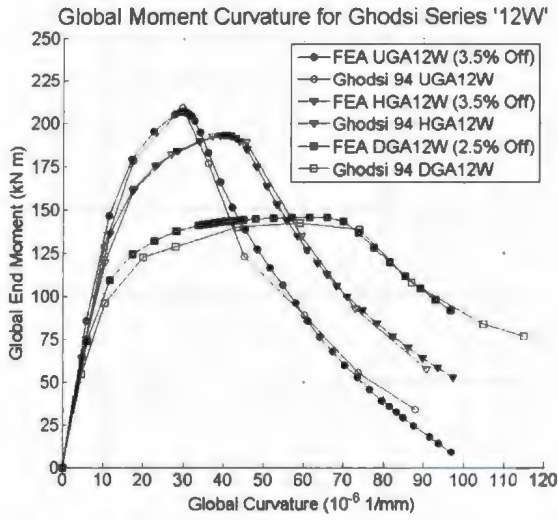


Figure 3-6: Calibration to Ghodsi et al. (1994)

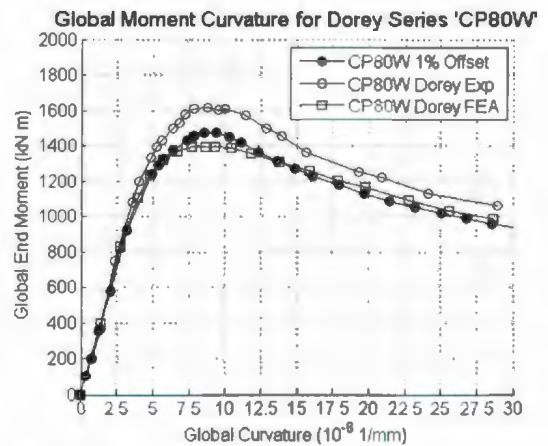
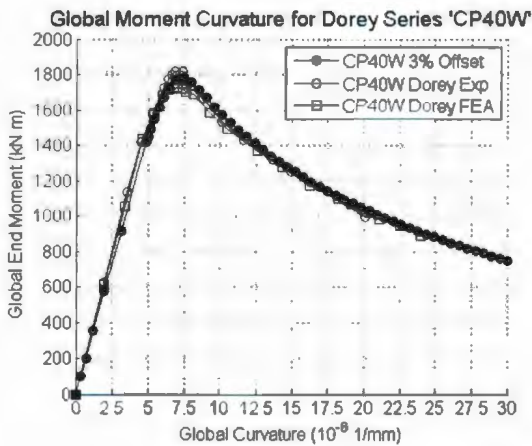
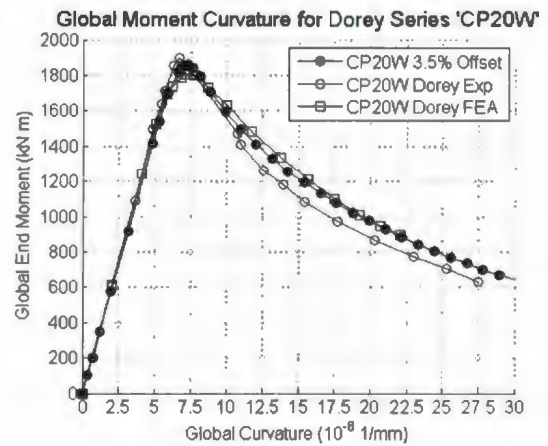
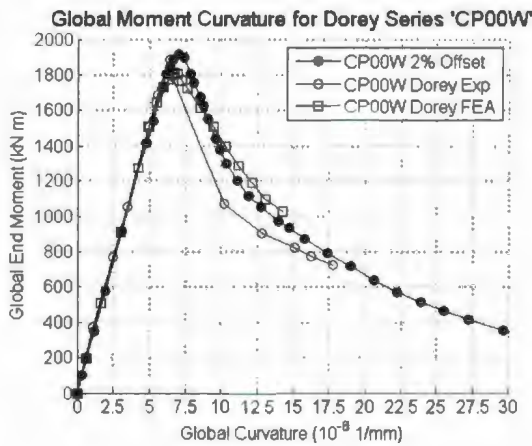


Figure 3-7: Calibration to Dorey (2001)

Most of the numerical results produced in OMAE 2009 study are consistent with the physical data with some exceptions. Ghodsi's reported some difficulties with the 20" diameter cases. During the initial test of UGA20W, control was lost for the loading jack and the data was abandoned because the pipe was plastically bent at the beginning of the test. Thus data from UGA20W-2 was reported. The shape of the moment curvature diagram produced by the calibration analysis for UGA20W-2 is consistent with that reported in Ghodsi et al. (1994), although the curvature is offset. This is likely due to similar difficulties reported in the physical experiment of UGA20W-2 as seen in UGA20W-1.

At high pressure, the pipeline system becomes inherently stiffer, thus requiring higher forces to bend and buckle the pipe. A potential explanation for the discrepancy between numerical and physical results seen in DGA20W (Figure 3-6) and CP80W (Figure 3-7) may be that part of the load is being carried by the testing frame and not the pipe section or, in the case of CP80W, "it is possible that the incorrect material properties were used as input into the FEA model for specimen CP80W" as stated in Dorey (2001). In spite of these discrepancies, the numerical model presented here is consistent with both physical test programs and finite element models presented by Dorey (2001) as shown in CP00W, CP20W and CP40W of Figure 3-7.

### **3.5. A PARAMETRIC ANALYSIS**

The OMAE 2009 parametric study was done to identify trends in the buckling capacity by varying five input parameters. These are: diameter (D), diameter to thickness ratio

(D/t), pressure-stress ratio ( $\beta$ ), axial load ratio (N) and initial imperfection amplitude. The axial load ratio refers to the load required to yield the pipe in the longitudinal direction, given in the equation (3-7).

$$N = \sigma_a / \sigma_y = F / A_s \sigma_y \quad (3-7)$$

Three values of the five parameters were considered resulting in a total of 243 analyses. Table 3-4 shows the range of parameters used in the parametric study.

	Low	Medium	High
Diameter (mm)	406.4	609.6	914.4
D/t <sub>n</sub>	30	60	90
Pressure Ratio, $\beta$	0.00	0.40	0.80
Axial Load Ratio, N	-0.30	-0.15	0.00
Imperfection Amplitude <sup>1</sup>	5% t <sub>n</sub>	10% t <sub>n</sub>	15% t <sub>n</sub>

<sup>1</sup> Amplitude limited to 3mm, maximum allowable from Table D-3 DNV (2000)

**Table 3-4: Analysis Matrix for Parametric Study**

The finite element mesh generation included end caps and collars, as in the calibration analysis, to avoid inconsistent end buckling modes, such as “elephant foot” buckles, as described by Dorey (2001). Pipe section length was kept constant at 3.5 diameters, where circumferential to axial mesh densities used were 60x143, 92x215, and 120x281 for 406.4mm, 609.6mm, and 914.4mm diameter pipes, respectively. As shell structures have closely spaced eigenvalues, the mesh density was selected to maintain consistent aspect ratio with element axial length of about 10mm. Generalized engineering stress-strain relationships used the Ramberg-Osgood formulation, as defined in Walker and Williams (1995), having specified yield strength of 483 MPa (X70).

### 3.6. RESULTS

Torselletti et al. (2005) made use of design equations in DNV (2000), for pipelines under internal overpressure, to normalize the data obtained from finite element results. The same approach is adopted here whereby most safety factors are assumed to be unity with the exception of:

- material resistance factor,  $\gamma_m$ , set to 1.15
- maximum allowed yield to tensile strength ratio,  $\alpha_h$ , set to 0.92
- girth weld factor,  $\alpha_{gw}$ , set to 0.9, 0.6, and 0.6 for D/t ratios 30, 60 and 90 respectively.

Thus, solving for  $M_{DNV}$  in equation (3-8) yields the normalization factor for critical moment obtained from the numerical analysis.

$$1.15 \left( \frac{F}{F_y} \right)^2 + 1.15 \frac{M_{DNV}}{M_{Plastic}} \sqrt{1 - \left( \frac{P}{P_y} \right)^2} + \left( \frac{P}{P_y} \right)^2 = 1$$

$$1.15(N)^2 + 1.15 \frac{M_{DNV}}{\sigma_y D_m^2 t_n} \sqrt{1 - (\beta)^2} + (\beta)^2 = 1 \quad (3-8)$$

The numerical critical global strain,  $\epsilon_g$ , calculated in equation (3-9), was normalized against the characteristic compressive strain,  $\epsilon_{DNV}$ , equation (3-10), where  $\alpha_h$  and  $\alpha_{gw}$  are listed above.

$$\epsilon_g = \kappa D \quad (3-9)$$

$$\epsilon_{DNV} = 0.78 \left( \frac{t_n}{D} - 0.01 \right) (1 + 5\beta) \alpha_h^{-1.5} \alpha_{gw} \quad (3-10)$$

The results of the parametric study are illustrated in Figure 3-8, Figure 3-9, and Figure 3-10 for D/t ratios of 30, 60 and 90, respectively. Each curve shown in the figures connects the variable of imperfection for each of the other test parameters. Surprisingly, there is little variation in the curves over the various diameters of pipe. Thus the three diameters are plotted together with the same line type and symbol. This convergence may be related to the classic buckling equation,  $\epsilon_{critical} = 1.2 t/D$ , or as an indication of stubby column buckling in the presence of an applied axial load since L/D is only 3.5. A general overall trend encompassing all D/t ratios is given in Figure 3-11 using a diameter of 609.6mm and an axial load ratio of 0.15.

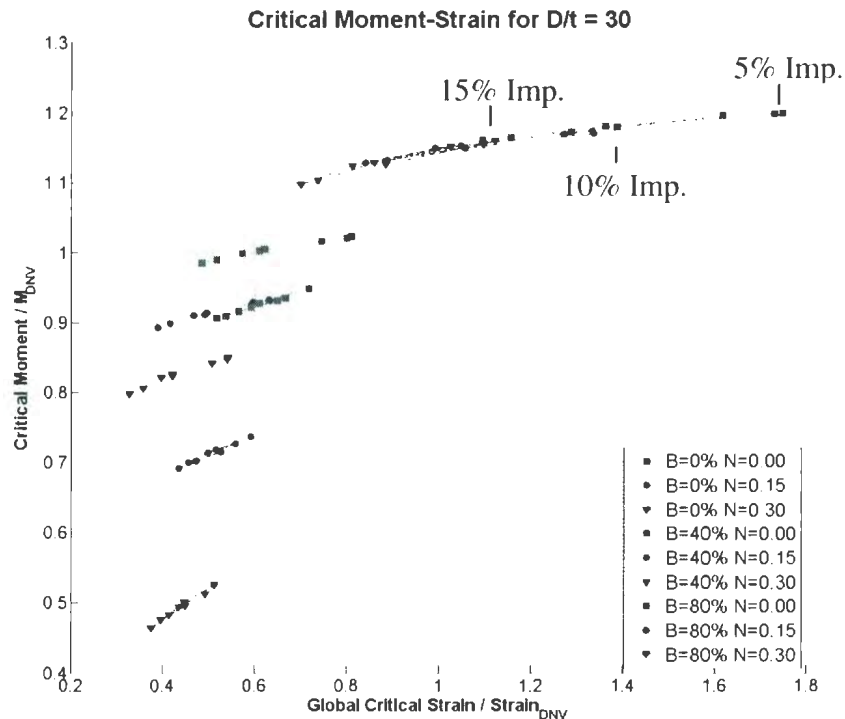


**Figure 3-8: Parametric Results – D/t = 30**

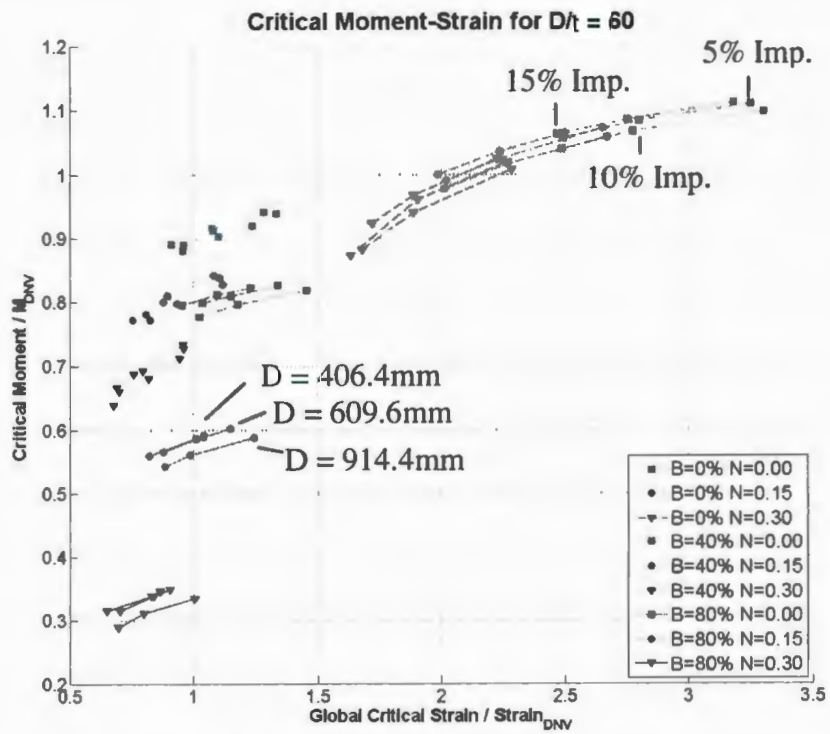


**Figure 3-9: Parametric Results –  $D/t = 60$**

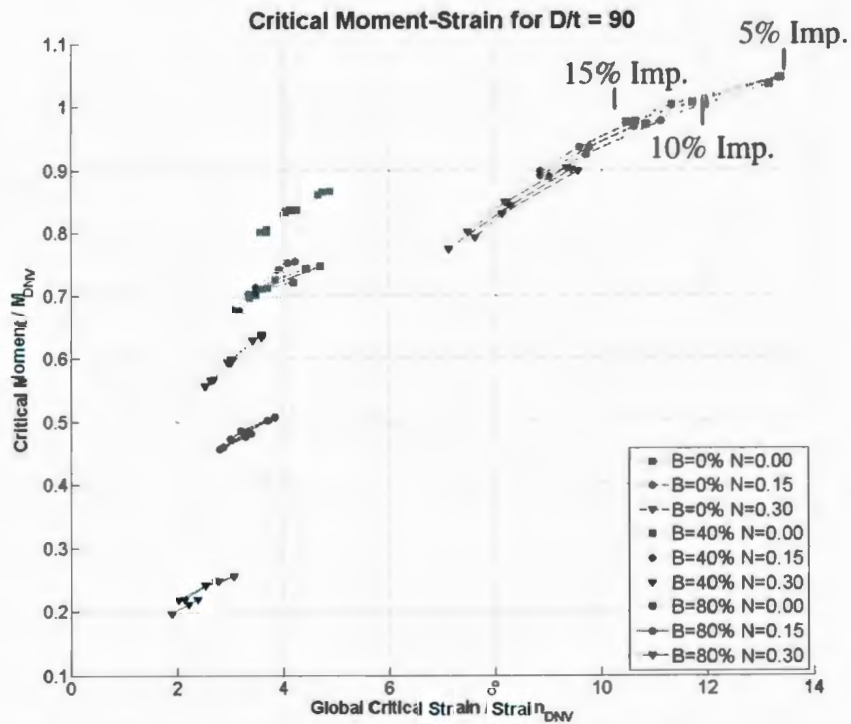


**Figure 3-10: Parametric Results –  $D/t = 90$**

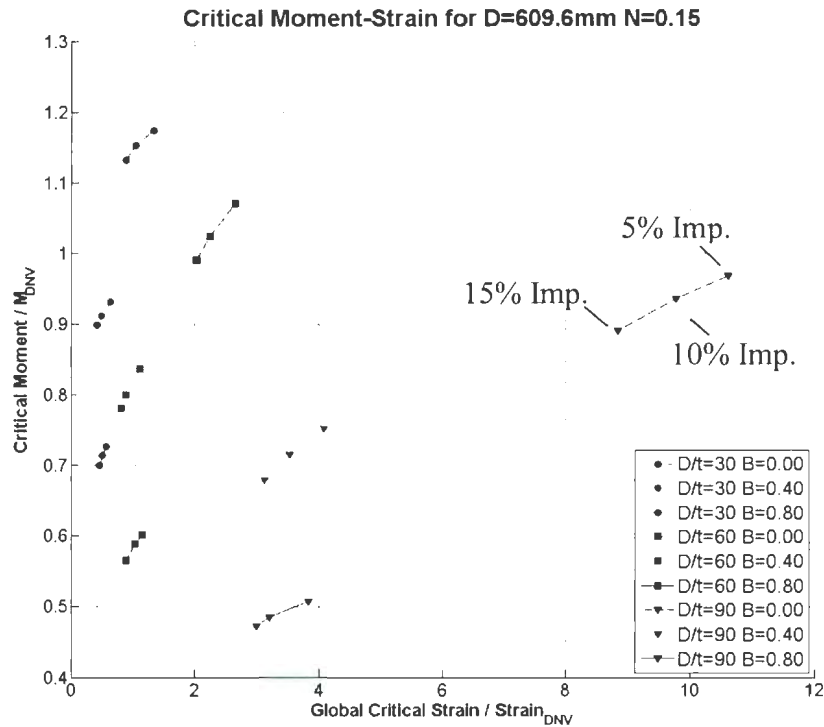


**Figure 3-11: Trend for D = 609.6mm, N = 0.15**

For the pure bending case and D/t ratios equal to 60, the findings in this paper are consistent with that of Torselletti et al. (2005). It is shown that the DNV (2000) equation for bending moment, axial force and internal overpressure for load control events appears to be slightly non-conservative for unpressurized pipes ( $M_{Critical} / M_{DNV} > 1$ ). Since the normalization did not account for other partial safety factors, the results are deemed to be within reasonable limits for engineering practice. The results for critical strain for these cases are consistent with Torselletti et al. (2005) as well and are generally conservative with the inclusion of a strain resistance factor of 2.6 on design strain, as stated in DNV.

However, including an applied axial load and pressure effects in combination has been shown to greatly reduce the strain and moment capacity of the pipeline. As shown in

Figure 3-8 for  $D/t = 60$ , the effect of applied pressure was to reduce the normalized moment by 0.5-0.6 and reduce normalized strain by 50%-55%. The degree of reduction for the normalized moment and strain due to applied axial force is dependant on the level of applied pressure. In the fully pressurized case,  $\beta=0.80$ , the moment ratio typically reduces by 0.5 while the strain ratio reduces by approximately 30%.

The effect of the girth weld misalignment amplitude was to reduce the peak bending moment capacity by 10% whereas strain capacity was reduced by as much as 35% based on the degree of girth weld imperfection.

On assessment of results for  $D/t$  ratios equal to 90, it readily becomes apparent that the DNV design equations, developed for  $D/t$  ratios less than 45, dramatically under predict global critical strains. This approach is not appropriate for design of pipelines with  $D/t$  ratios equal to 90, but is presented here for completeness.

Finally, strain behaviour over various pressure levels is shown to be non-linear. It may be difficult to capture this behaviour in a single design equation since the mode of buckling changes drastically given the pressure level.

### **3.7. CONCLUSIONS**

The calibrated finite element model presented in this paper has been shown to be consistent with several physical experiments over a range of design parameters. This

modeling procedure was then applied parametrically over five design parameters and has yielded very interesting results.

The analysis of the parametric study has shown that:

- An increased axial force decreases critical moment as well as critical strain by as much as 40% and 50% for both moment and strain, respectively.
- The degree of imperfection has been shown to reduce the moment and strain capacities by about 10% and 35% for moment and strain, respectively.
- Strain behaviour over various pressure levels is non-linear. It may be more suitable to develop a failure surface dependant on the buckling mode of the pipe.

## **ACKNOWLEDGMENTS**

Time and support from C-CORE is greatly appreciated.

## **NOMENCLATURE**

$A_s$	Cross Sectional Area of Steel
$D$	Outside Diameter
$D_m$	Mean Diameter
$E$	Elastic Modulus
$F$	Applied Axial Force
$F_y$	Force to Yield Pipe Section Axially
$h_{\text{offset}}$	Measured Distance From End Cap to Reference Point
$L$	Pipe Length

LPF	Load Participation Factor
$M_{DNV}$	DNV (2000) Design Moment
MPC	Multi-Point Constraint
NPS	Nominal Pipe Size
P	Applied Pressure
$P_y$	Pressure to Yield Pipe Section Circumferentially
$t_n$	Nominal Wall Thickness
$\Delta T$	Change in Temperature
$\alpha$	Coefficient of Thermal Expansion
$\alpha_{gw}$	Girth Weld Factor
$\alpha_h$	Maximum Allowed Yield to Tensile Strength Ratio
$\beta$	Pressure Stress Ratio
$\epsilon_{DNV}$	DNV (2000) Characteristic Strain
$\kappa$	Global Curvature
$\nu$	Poisson Ratio
$\theta$	Rotation Measured at Reference Point
$\sigma_a$	Axial Stress
$\sigma_h$	Circumferential (Hoop) Stress

### 3.8. REFERENCES

- Al-Showaiter, A., Taheri, F., and Kenny, S. (2008). "Influence of Pipeline Misalignment on the Local Buckling Response. International Pipeline Conference 2008". September 29 – October 3, Calgary, Alberta, Canada.
- DNV OS-F101 (2000). "Submarine Pipeline Systems". Det Norske Veritas.
- Dorey, A. (2001). "Critical Buckling Strains in Energy Pipelines". Doctoral Thesis. University of Alberta Department of Civil Engineering, Structural Engineering.
- Ghodsi Nader Yoosef-, Kulak G. L. and Murray D. W. (1994). "Behaviour of Girth Welded Line-Pipe". University of Alberta Department of Civil Engineering, Structural Engineering. Report No. 23.
- Mohareb, M. E., Elwi, A. E., Kulak, G. L., and Murray, D. W. (1994). "Deformational Behaviour of Line Pipe". Structural Engineering Report No. 202, Department of Civil Engineering, University of Alberta, Edmonton, Alberta.
- Mohareb, M., Kulak, G. L., Elwi, A., and Murray, D. W. (2001). "Testing and Analysis of Steel Pipe Segments". Journal of Transportation Engineering. Vol 127, No. 5, September/October 2001. pp. 408-417.
- Torselletti, E., Vitali, L., and Bruschi, R. (2005). "Bending Capacity of Girth-Welded Pipes". Proceedings of the 24th OMAE. Halkidiki, Greece.
- Walker, A. C. and Williams, K. A. J. (1995). "Strain Based Design of Pipelines". Proceedings of OMAE, Vol.V, pp. 345-350.

## **4. CSCE 2009 – INVESTIGATION ON THE BUCKLING BEHAVIOUR OF GIRTH WELDED PIPELINES**

*Submitted to: 1st International / 1st Engineering Mechanics and Materials Specialty  
Conference*

*Authors: John Barrett, Shawn Kenny and Ryan Phillips*

*Reviewed and Accepted on: March 7, 2009*

### **4.1. SYNOPSIS**

Further reduction of the data produced from the parametric study described in Chapter 3 focused on the assessment of buckled wave form patterns, ovality and the influence of the total length of the pipe section on the global buckling response of the girth welded section.

It was shown in the following CSCE 2009 paper that the buckled profile of the test section is primarily affected by diameter, diameter to thickness ratio and pressure. Increasing  $D/t$  ratio, results in a decrease in the critical wavelength and amplitude required to trigger buckling. This is consistent with the works of Ju and Kyriakides (1992) in their study of cylinders under axial and bending loads. Conversely, increasing pressure tended to increase wavelength and amplitude of the buckle showing correspondence to Kyriakides and Corona (2007) where they note an increase in the bifurcation wavelength due to increasing internal pressure. The other design parameters studied, applied compressive axial load and misalignment amplitudes, were found to

simply shift the value of critical buckling strain and have little effect on the buckled shape.

Ovality was shown to be influenced by diameter to thickness ratio and pressure and to a lesser degree, by applied axial load and imperfection. Ovality remained constant over the range of diameters studied.

The following CSCE 2009 paper has shown that end effects are enhanced by pressurizing pipes, which was shown to be a direct result of the length of the pipeline. While the length of the pipeline in this study was set to 3.5 diameters to simulate experimental conditions, the buckled wavelengths show a great degree of interference between the central buckle and buckles developed at the ends of the pipe. This paper recommends that in further study, either physical or numerical, should consider pipe sections at a minimum of 5 to 6 diameters in length.

#### **4.2. ABSTRACT**

The ultimate goal in pipeline design is to minimize material costs without jeopardizing the integrity of the pipeline system. A greater level of understanding of pipeline deformation behaviour and more sophisticated analysis tools are required when considering extreme loads and large deformation.

The Finite Element Method (FEM) has been used to assess the bending moment and strain capacity of pipeline under typical design condition and parameters. After the

analysis was calibrated to physical data, this study investigated buckled profiles and ovality with respect to critical bending response of girth welded pipelines over a range of typical design parameters. These parameters included diameter, thickness, internal pressure, applied axial load and degree of misalignment.

The results of this study have indicated that the buckled wave form observed in the profile of the pipelines is primarily affected by diameter, diameter to thickness ratio and pressure with applied compressive axial load and misalignment having lesser effects. Ovality has been shown to be influenced by diameter to thickness ratio and pressure. Ovality is affected to a lesser degree by applied axial load and imperfection. However, ovality has been shown to remain constant over the range of diameters studied.

End effects were discovered to be a problem when considering pressurized pipes. This has been shown to be a direct result of the length of the pipeline. While the length of the pipeline in this study was set to 3.5 diameters to simulate experimental conditions, the buckled wavelengths show a great degree of interference between the central buckle and buckles developed at the ends of the pipe. It has been recommended that in further study, at a minimum, the length of the pipeline be increased to five to six diameters.

### **4.3. INTRODUCTION**

This paper details the investigation of buckling behaviour of the pipeline section subject to combined loading. The purpose of this study is to provide a better understanding of buckling mechanisms and failure under non-linear and large deformation common

extreme loading events. Since a Finite Element Method (FEM) of analysis was adopted for this assessment, the numerical model was calibrated to physical data. The model was then used over a range of pipeline diameters, thickness, internal pressure, applied axial load and misalignment amplitudes to identify trends in the data. Of particular interest were buckled wavelength profiles and distributions of ovality of girth welded pipelines. Since the effects of material strength and material anisotropy were not part of this study, isotropic standard X70 steel was used for all analysis.

#### 4.4. CALIBRTION OF NUMERICAL MODEL

Ghodsi et al. (1994) and Dorey (2001) investigated the effects of girth welds on the buckling behaviour of pipelines. Ghodsi et al. (1994) developed a physical test program considering 324mm and 508mm pipelines of grade X52 and X56, respectively, at the pipeline testing facility at the University of Alberta. The pipelines were tested at three different pressure levels (pressurized, unpressurized and at a 50% pressurized level) where the pipeline segment was girth welded at midspan. Dorey (2001) conducted a series of physical experiments for girth welded pipe as well for 762mm pipe, having specified yield strength of grade X70, over four different pressures (P). These tests were denoted as CP##W, where ## represented 0, 20, 40 and 80% pressure to cause yield in the circumferential direction of the pipe section, defined by the pressure-stress ratio  $\beta$ , which is given in equation (4-1).  $D_m$  and  $t_n$  represent mean diameter and nominal wall thickness, respectively.

$$\beta = \sigma_{\text{Hoop}} / \sigma_{\text{yield}} = (P D_m / 2t_n) / \sigma_{\text{yield}} \quad (4-1)$$

In addition, Dorey developed a numerical procedure to capture his own physical tests as well as the experiments conducted by Ghodsi et al. (1994) and Mohareb et al. (1994).

The calibration analysis conducted for the OMAE 2009 and CSCE 2009 studies made use of both Ghodsi et al. (1994) and Dorey (2001) results using ABAQUS v6.7. A Multi-Point Constraint (MPC) was used to tie the circumferential nodes at the end of the pipe to a single reference node. The reference node then becomes the pivot point for the applied bending moment and axial force. The MPC used in this analysis does not, however, allow for the end section to ovalize. An illustration of the developed finite element model is given in Figure 4-1.

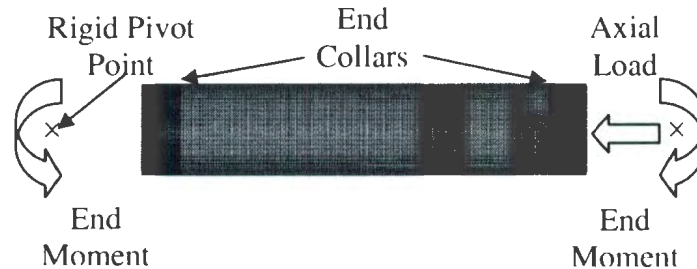


**Figure 4-1: Finite Element Schematic**

The nonlinear solver used for the buckling analysis was the Modified Riks Method. The Load Participation Factor (LPF) from the solution technique was used to calculate the applied end moments ( $M_{End}$ ). Second order effects arising from the applied axial force ( $F_{Axial}$ ) were also accounted for, modified slightly from Mohareb et al. (2001), using the following equation (4-2),

$$M_{End} = M_{LPF} + F_{Axial} h_{Offset} \sin(\theta_1) \quad (4-2)$$

where  $h_{\text{Offset}}$  is the distance from the end cap to the rigid reference point and  $\theta_1$  is the measure of rotation at the pivot point. Global curvatures ( $\kappa$ ) were calculated based on the differential rotation ( $\Delta\theta_{\text{Ends}}$ ) measured at the reference points over the pipe sections total length ( $L$ ) as indicated by equation (4-3).

$$\kappa = \Delta\theta_{\text{Ends}} / L \quad (4-3)$$

A 4-noded shell element, with reduced integration and hourglass control (element S4R), was used as its formulation allows for large displacement and finite membrane strain. The circumferential to longitudinal mesh densities used in the calibration analysis of 324mm and 508mm pipe were 60 to 161, consistent with the density used in Al-Showaiter et al. (2008). The mesh density used for the 762mm pipe was 40 to 75, as used in Dorey (2001). Two end collars that were used in the physical experiment, as well as the end caps, were modelled numerically. Both collars were 150mm in length and had the same thickness as the pipe section being analyzed. Some of the results of the calibration analysis are shown in Figure 4-2 for Ghodsi et al. (1994) and Dorey (2001).

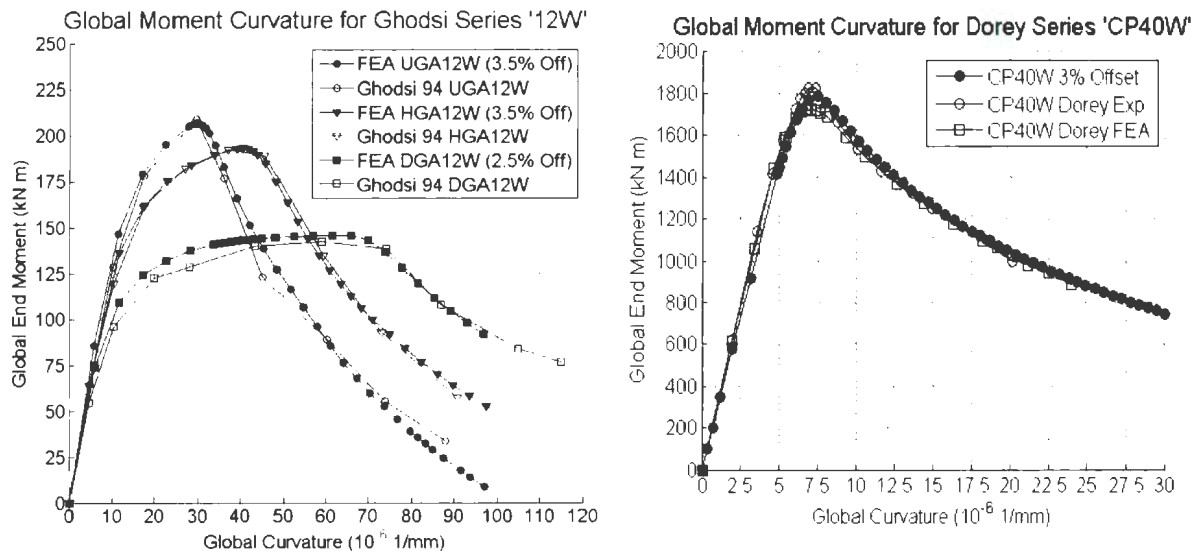


**Figure 4-2: Calibration to Ghodsi et al. (1994) and Dorey (2001)**

A summary table of the calibration analyses is given in Table 4-1 whereas Table 4-2 indicates the true stress-strain material data used.

	Ghodsi (1994)						Dorey (2001)
	UGA12W	HGA12W	DGA12W	UGA20W	HGA20W	DGA20W	CP40W
D (mm)	324	324	324	508	508	508	762
$t_n$ (mm)	6.35	6.35	6.35	7.9	7.9	7.9	8.3
$D/t_n$	51	51	51	64	64	64	92
L (m)	1.69	1.69	1.69	1.69	1.69	1.69	2.7
$\beta$	0.00	0.36	0.72	0.00	0.40	0.80	0.40
P (MPa)	0.00	5.26	10.52	0.00	4.96	9.91	4.30
Grade	X52	X52	X52	X56	X56	X56	X70
$h_{Offset}$ (mm)	162	162	162	254	254	254	381
F (kN)	667	822	978	1333	1701	2069	2806

**Table 4-1: Input Parameters for Calibration Study**

X52		X56		X70	
<u>Stress (Pa)</u>	<u>Strain (-)</u>	<u>Stress (Pa)</u>	<u>Strain (-)</u>	<u>Stress (Pa)</u>	<u>Strain (-)</u>
0.00E+00	0.00000	0.00E+00	0.00000	0.00E+00	0.00000
2.00E+08	0.00100	2.00E+08	0.00100	5.68E+08	0.00279
3.29E+08	0.00194	3.31E+08	0.00192	5.77E+08	0.01065
3.75E+08	0.00241	3.75E+08	0.00238	5.88E+08	0.02073
3.92E+08	0.00476	3.87E+08	0.00376	6.01E+08	0.03339
4.05E+08	0.01041	3.94E+08	0.00468	6.12E+08	0.04772
4.16E+08	0.02029	4.05E+08	0.01020	6.23E+08	0.06473
4.35E+08	0.03959	4.18E+08	0.02031	6.32E+08	0.08125
4.49E+08	0.05794	4.34E+08	0.03962	6.37E+08	0.10290
4.64E+08	0.07677	4.49E+08	0.05847		
5.21E+08	0.18218	4.62E+08	0.07732		
		5.19E+08	0.18261		

**Table 4-2: Calibration True Stress-Strain Definition**

#### 4.5. THE PARAMETRIC ANALYSIS

A parametric study was done, Barrett et al. (2009), to identify trends in the buckling capacity by varying five input parameters. These are diameter (D), diameter to thickness ratio (D/t), pressure-stress ratio ( $\beta$ ), axial load ratio (N) and misalignment imperfection amplitude. The axial load ratio refers to the load required to yield the pipe in the longitudinal direction, given in the equation (4-4).

$$N = \sigma_{axial} / \sigma_{yield} = F_{Axial} / A_s \sigma_{yield} \quad (4-4)$$

Three levels of the five parameters were considered resulting in a total of 243 analyses. Table 4-3 shows the range of parameters used in the parametric study.

	Low	Medium	High
Diameter (mm)	406.4	609.6	914.4
D/tn	30	60	90
Pressure Ratio, $\beta$	0.00	0.40	0.80
Axial Load Ratio, N	-0.30	-0.15	0.00
Imperfection Amplitude <sup>1</sup>	5% tn	10% tn	15% tn

<sup>1</sup> Amplitude limited to 3mm, maximum allowable from Table D-3 DNV (2000)

**Table 4-3: Analysis Matrix for Parametric Study**

The pipe section length was kept at a constant at 3.5 diameters, where circumferential to axial mesh densities used were 60x143, 92x215, and 120x281 for 406.4mm, 609.6mm, and 914.4mm diameter pipes, respectively. The mesh density was selected to maintain a consistent aspect ratio with an element axial length of about 10mm. Generalized engineering stress-strain relationships used the Ramberg-Osgood formulation, as defined in Walker and Williams (1995), having specified yield strength of 483 MPa (X70).

#### **4.6. BUCKLED WAVE FORM AMPLITUDE AND LENGTH**

Buckled profiles were assessed to identify the effects of the five parameters on the mode and shape of buckling. Key results of interest were critical buckling amplitude, wavelength and number of waves across the test section. By estimating the global curvature radius, based on equation (4-3), and drawing an arc passing through the ends of the pipeline, the dominant global single sinusoidal waveform can be removed from the buckled shape revealing local superimposed waveforms. This concept is illustrated in Figure 4-3 where  $\delta R$  illustrates the variation from global curvature and the vertical line on the moment strain diagram indicates the strain level of the buckled profile.

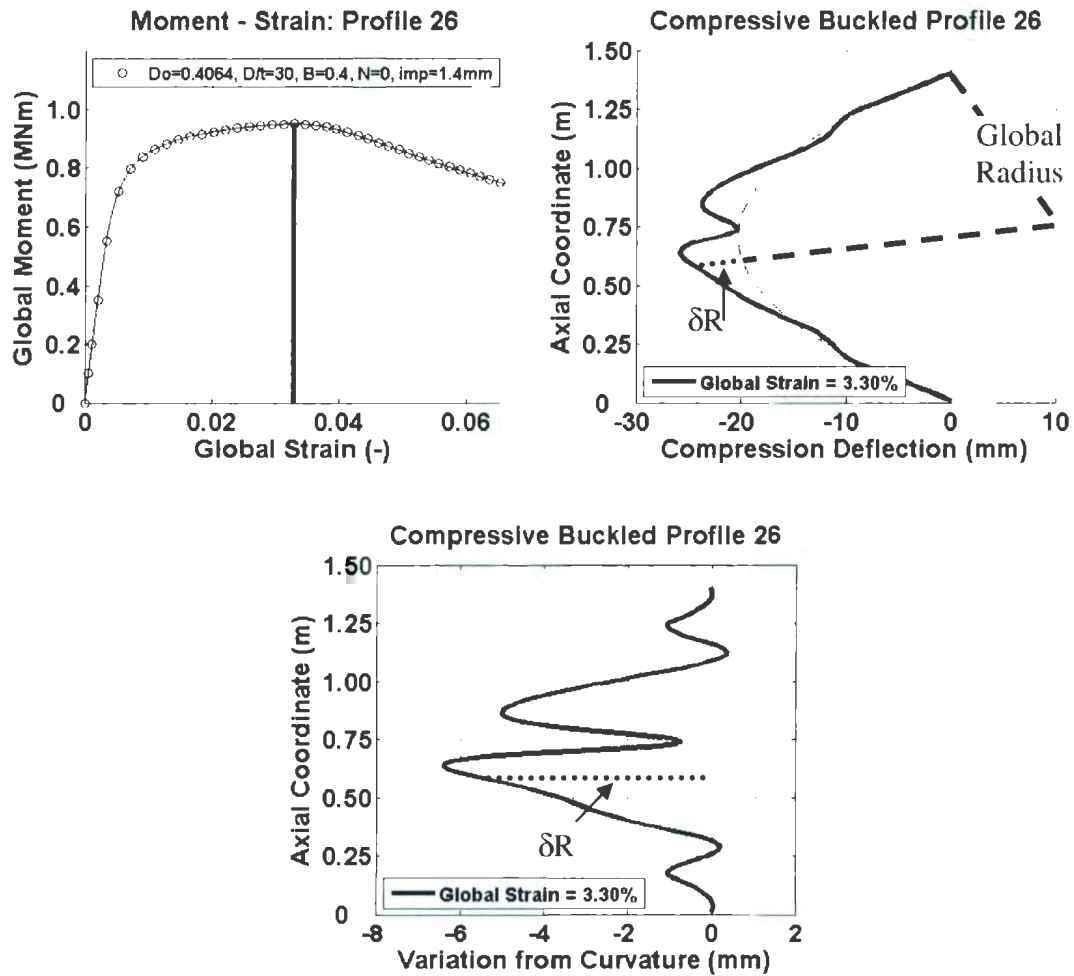


**Figure 4-3: Measuring Variation from Global Curvature**

Using this concept, the buckled shape from the parametric study was analyzed at the critical point of buckling and it was found that:

- Decreasing diameter decreases both wavelength and amplitude.
- Increasing  $D/t$  results in a decrease in the wavelength and amplitude required to trigger buckling. This is consistent with the works of Ju and Kyriakides (1992) in their study of cylinders under axial and bending loads.

- Increasing the pressure results in an increase in both the wavelength and amplitude of the buckle. This is shown in Kyriakides and Corona (2007) where they have noted that an increase in the bifurcation wavelength with increasing design factor (i.e. internal pressure) for problems involving plastic buckling response for axial compression.
- The effect of compressive applied axial load for the parameter range examined had little effect on the wavelength and amplitude of the buckle.
- Amplitude of misalignment does not affect amplitude or wavelength of buckle.

Further, the wavelength of the buckled shape remained relatively constant and the wave increased in amplitude only with further end rotation. Unfortunately, it was observed for some of the fully pressurized cases, as shown in Figure 4-3, additional wave forms develop near the collars having significant wavelengths and amplitudes compared with the central buckling mode. There are approximately eight half-wave forms shown for this case.

Though the majority results displayed a central buckle, fully pressurized cases having imperfection misalignment of  $5\% t_n$  resulted in either a single or double end buckle, the later being characteristic of perfect pipe buckling. This is an indication that the central girth weld imperfection is not great enough to overcome the end effects. In pressurized cases, end effects are present to some degree up to the critical buckling point. Once the

dominant central wave form triggered the buckle, wave forms at the ends relax in amplitude post-peak critical moment.

#### 4.7. CRITICAL OVALITY

Ovality of a pipe is a measure of deviation of the pipe's section from a perfect circular section. DNV (2000) defines a normalized ovality ( $f_0$ ) according to equation (4-5):

$$f_0 = (D_{\text{Max}} - D_{\text{Min}}) / D_M \quad (4-5)$$

Ovality measurements were recorded at the girth weld as well as 0.5D, 0.75D and 1D on both sides of the girth weld for a total of 7 measurements over all strains during the buckling event. The ovality measured at the critical strain was plotted against distance from the girth weld to show the profile of ovality as well as trends across the various parameters. An example is shown in Figure 4-4.

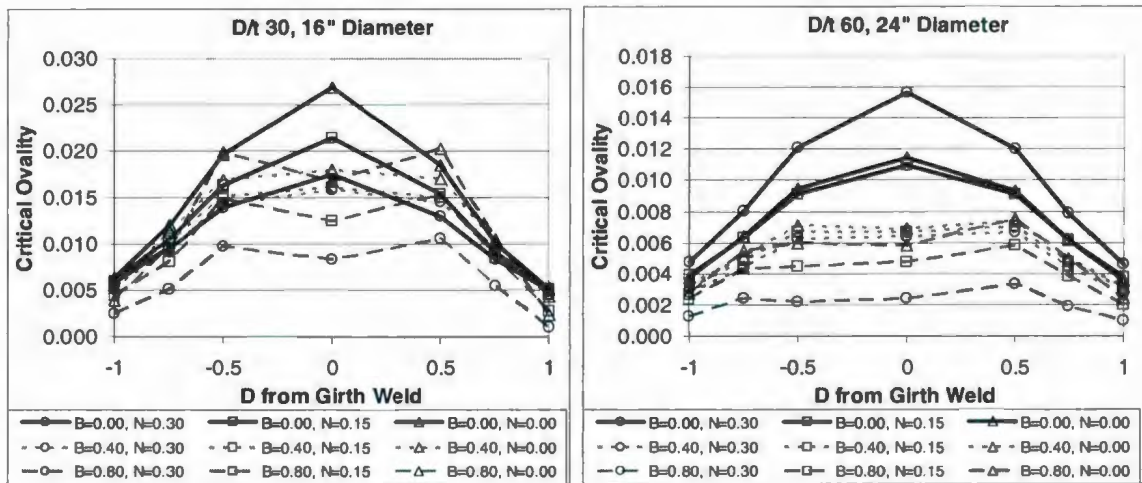


Figure 4-4: Critical Ovality Measurement

It was found that:

- Ovality remains relatively constant over changes in diameter (Figure 4-5).

- Ovality increases with decreasing  $D/t$  ratio (Figure 4-6).
- Ovality decreases with increasing pressure (Figure 4-7).
- As a result of decreasing critical strain, applied axial load changes the location of the onset of the nonlinear portion of ovality. Linear portions remain constant (Figure 4-8).
- The amplitude of misalignment alters the onset of buckling, not the measure of ovality (Figure 4-9), having a similar effect as the applied axial load.

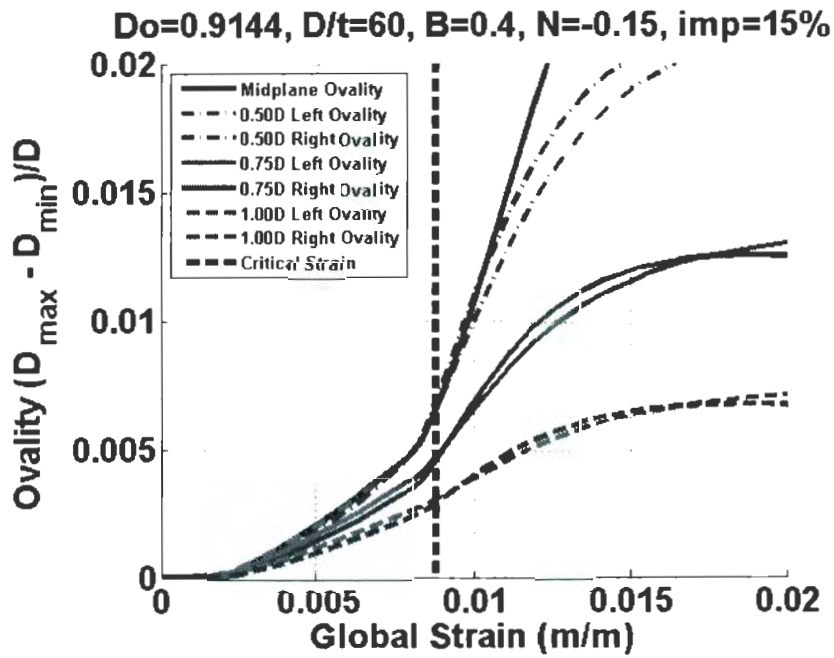
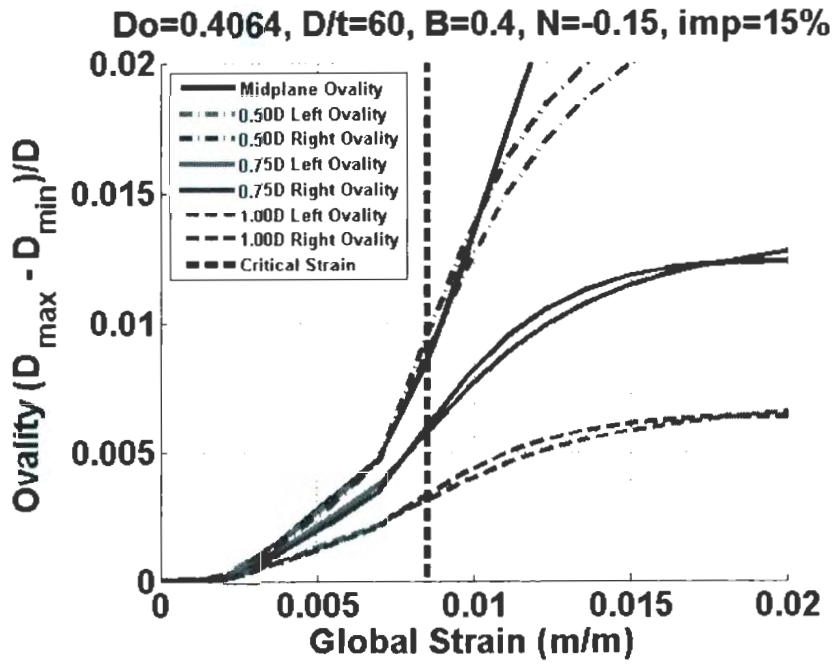


Figure 4-5: Ovality Measurement for Diameter

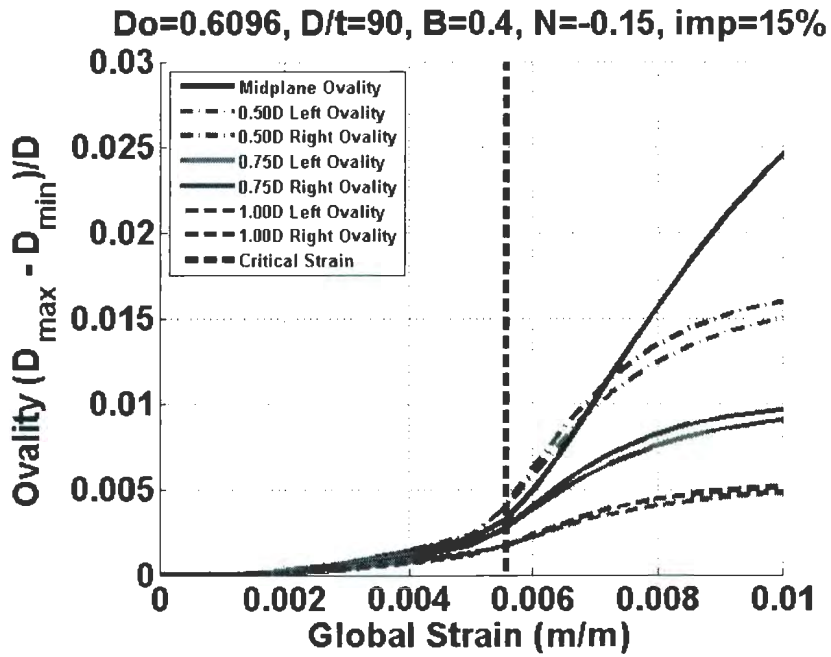
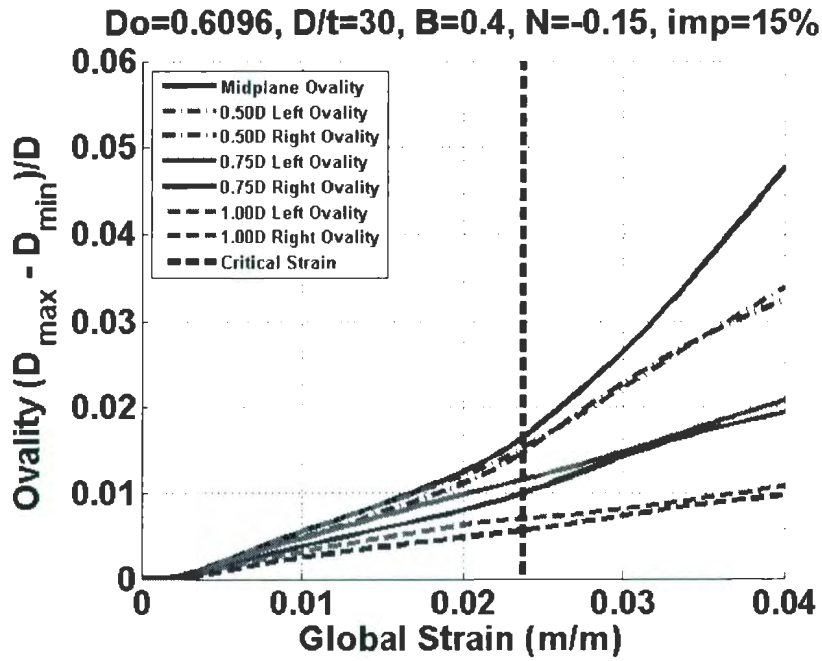
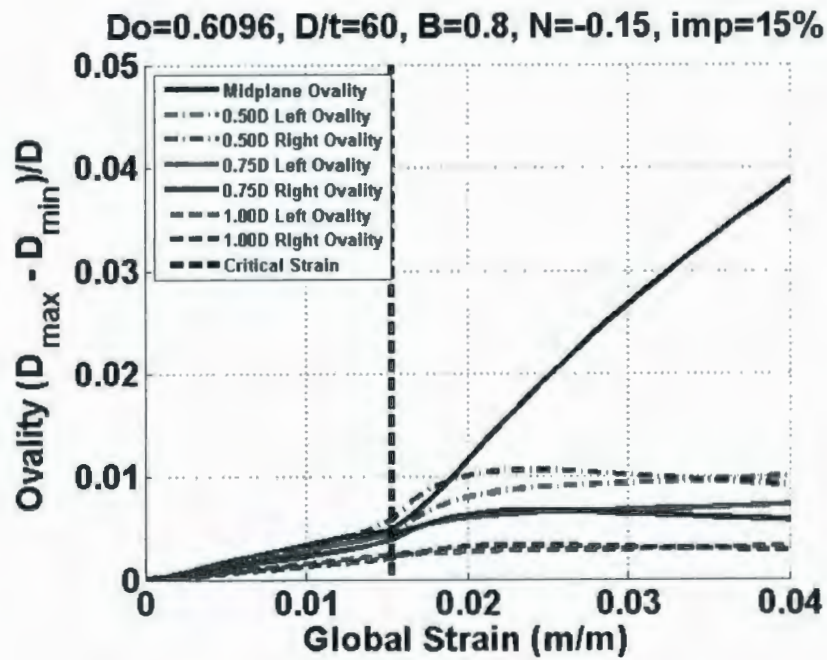
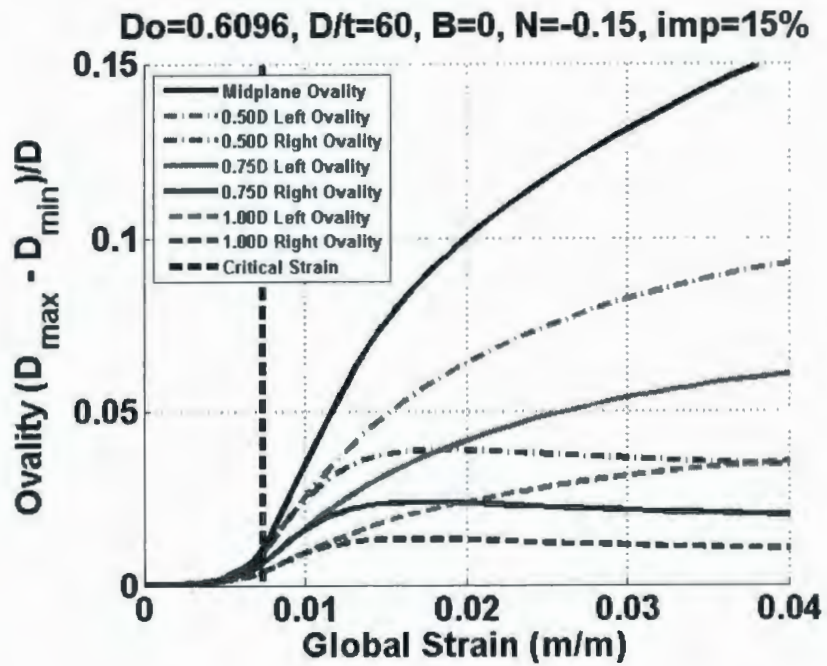


Figure 4-6: Ovality Measurement for D/t Ratio



**Figure 4-7: Ovality Measurement for Pressure Ratio**

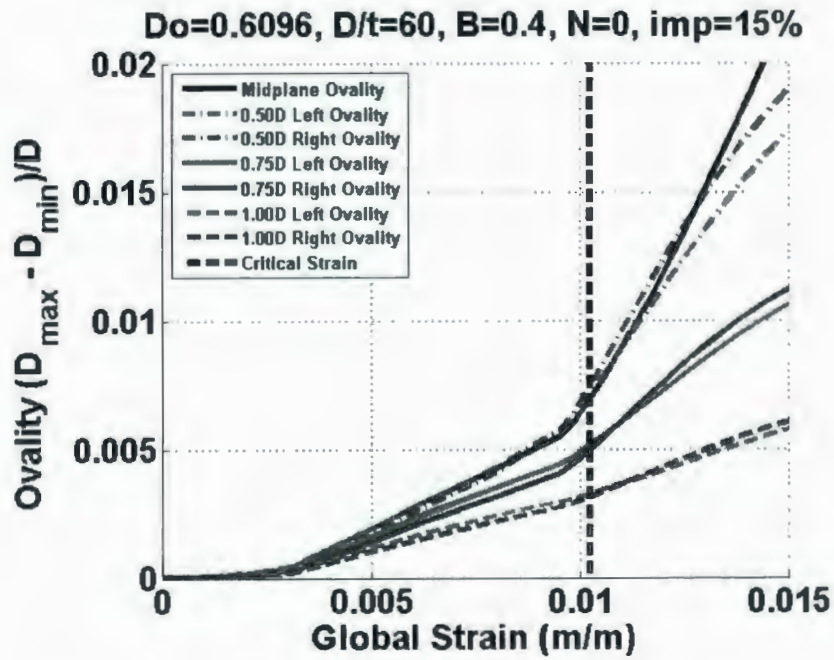
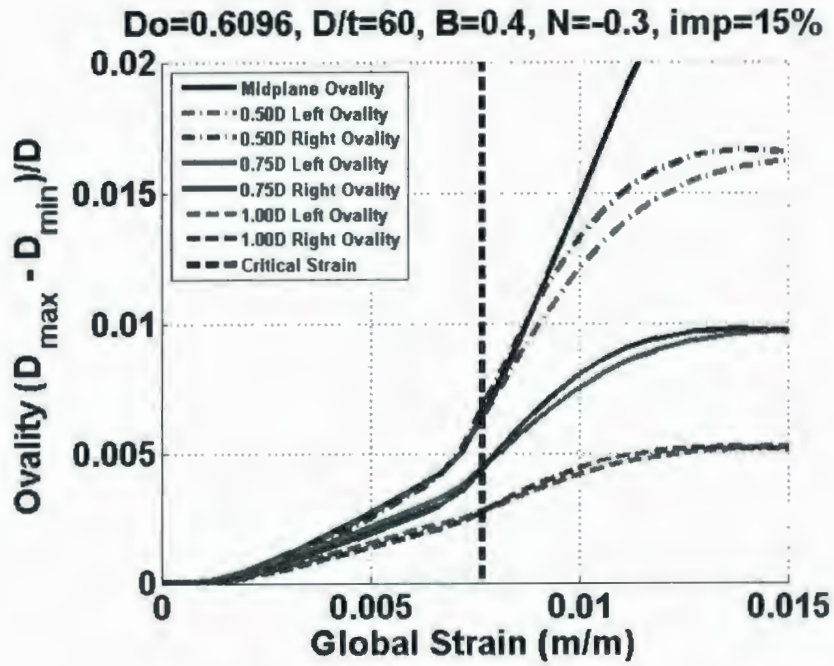
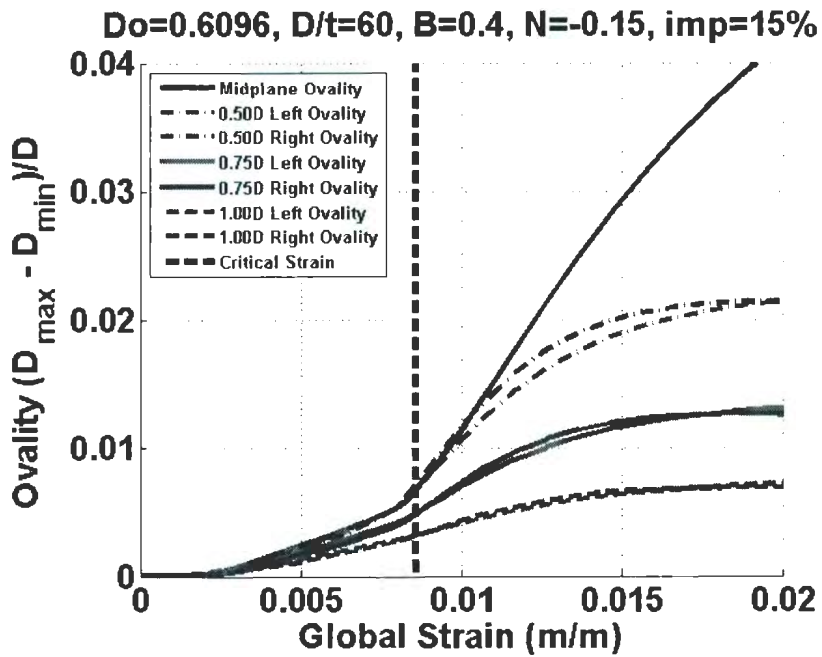
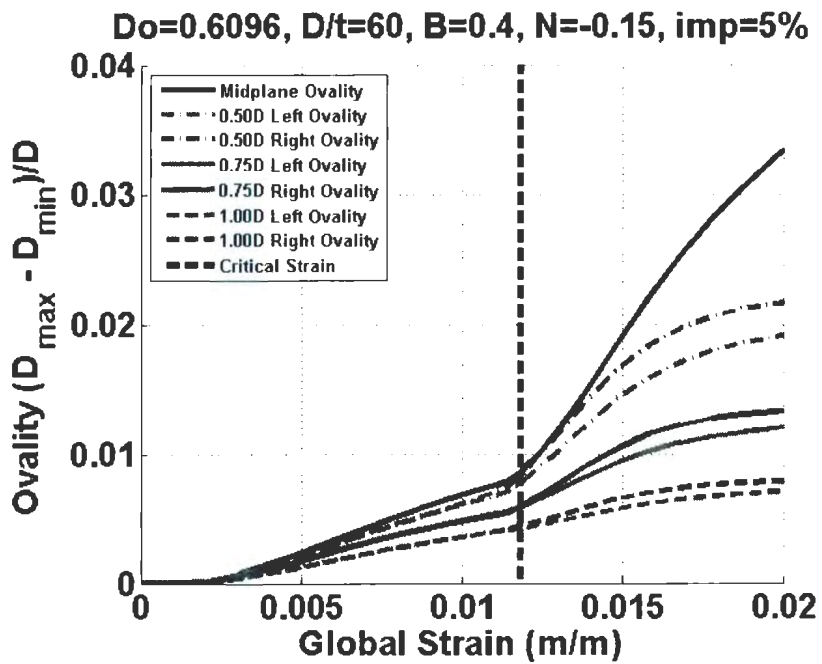


Figure 4-8: Ovality Measurement for Axial Load Ratio



**Figure 4-9: Ovality Measurement for Misalignment**

#### 4.8. L/D DISCUSSION

In experiments conducted by Ghodsi et al. (1994) and Dorey (2001), the purpose of the end collars was not only to restrain the pipe, but also to mitigate boundary effects interfering with the experiment. It was discovered in the study of buckled wavelength and shape, that some of the analysis developed significant deformation amplitudes near the collars of the pipe section. As shown in Figure 4-10, high pressure pipes are particularly susceptible to end buckles. It is not surprising end buckles arise in a physical test since the slightest imperfection or stress concentration at the ends will trigger a buckle away from the girth weld.

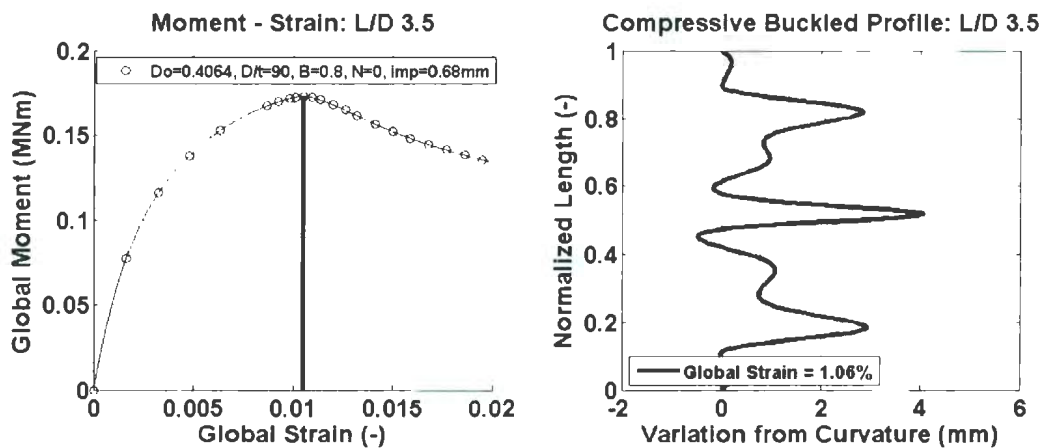


**Figure 4-10: Buckled Profile for L/D = 3.5**

At a length to diameter ratio ( $L/D$ ) of 3.5, the preferred wavelengths located at the centre and ends of the fully pressurized pipes are of sufficient length to interfere with each other. This interference results in an over-prediction of peak moment and strain capacity as the buckled mode shape tends towards buckling of a geometrically perfect pipe. Additional analyses were carried out using  $L/D$  ratios of 5.5 (similar to UGA12W in

calibration analysis) and 10 for cases in the parametric analysis where end effect wave forms were significant in comparison to the central buckle. It was found that by increasing the length to diameter ratio, the influence of end effects decrease proportional to  $L/D$ . The relative magnitude of end effect wave amplitude to girth weld wave amplitude was found to be 0.75, 0.5 and 0.3 for  $L/D$  of 3.5, 5.5 and 10, respectively. Critical deformation profiles and variation from global curvature diagrams are given for these cases in Figure 4-10 to Figure 4-12 where variation in curvature is plotted against normalized length (Total Length / Number of Diameters).

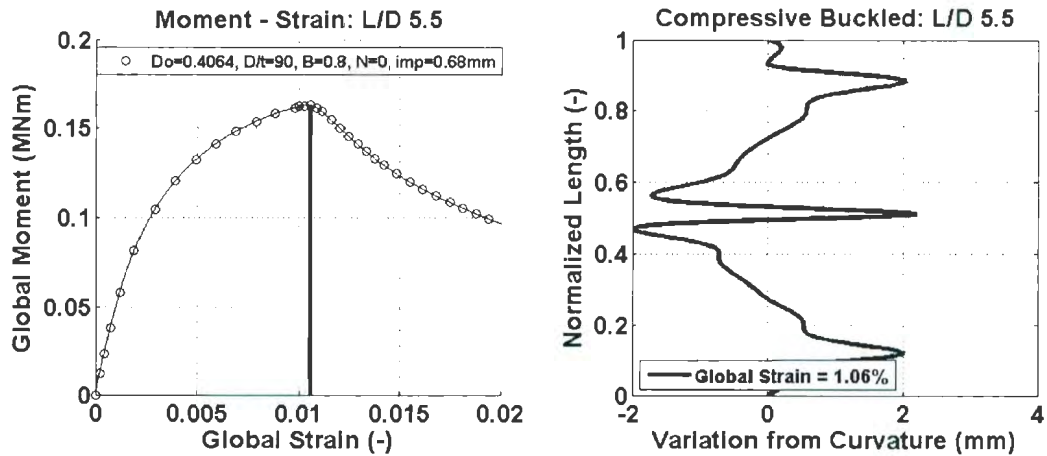


Figure 4-11: Buckled Profile for  $L/D = 5.5$

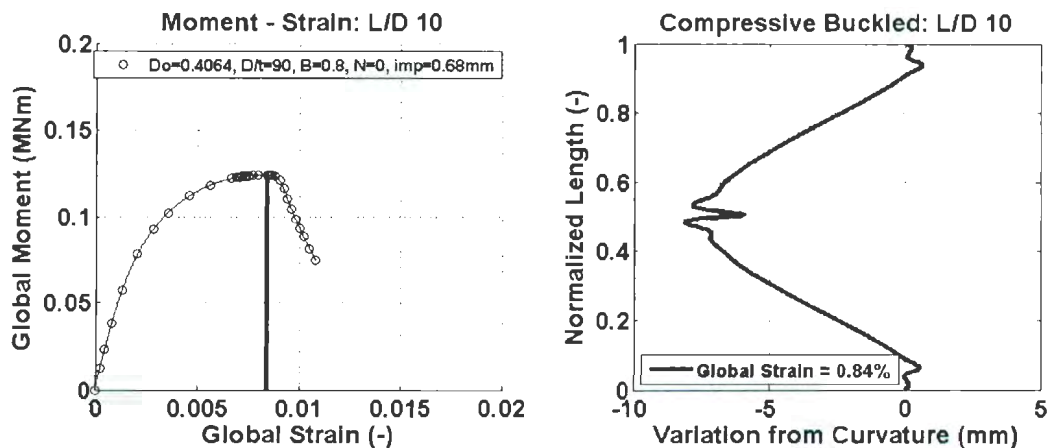


Figure 4-12: Buckled Profile for  $L/D = 10$

#### **4.9. CONCLUSIONS**

Through calibration with full-scale data, a finite element model has been used to assess practical pipeline design parameters through parametric numerical study. By analysing buckled profiles, it was determined that the main factors affecting buckled wavelength and amplitude were pipeline diameter, diameter to thickness ratio and applied internal pressure, whereas applied compressive axial load and imperfection amplitude tended to shift the buckling point not the wave form of deformation. Similar observations were made about ovality measured at the peak moment. Ovality was found to remain constant over diameter, increase with decreasing  $D/t$ , decrease with internal pressure, and remain unaffected by axial force or amplitude of imperfection.

End effects were illustrated for fully pressurized pipes having a length equal to 3.5 diameters. This has given insight into the problems seen in the physical testing of these pipes. In these cases, the buckled wavelengths show a great degree of interference. Due to this interference, peak moment and strain capacities are over predicted as the buckled wave form approaches the geometrically perfect pipe buckling mode. It is recommended that further study in this area involve pipe lengths, at minimum, 5 to 6 diameters in length.

#### **ACKNOWLEDGMENTS**

Research conducted for this study was done by the lead author in partial requirement of a Master's degree in Engineering at Memorial University of Newfoundland.

Acknowledgements are extended to C-CORE for the time and support afforded in this endeavour.

#### **4.10. REFERENCES**

- Al-Showaiter, A., Taheri, F., and Kenny, S. (2008). "Influence of Pipeline Misalignment on the Local Buckling Response". International Pipeline Conference 2008. September 29 – October 3, Calgary, Alberta, Canada.
- Barrett, J., Kenny, S. and Phillips, R. (2009). "Effects of Girth Weld on the Local Buckling Response of Conventional Grade Pipelines". 28th International Conference of OMAE. In Press.
- DNV OS-F101 (2000). "Submarine Pipeline Systems". Det Norske Veritas.
- Dorey, A. (2001). "Critical Buckling Strains in Energy Pipelines". Doctoral Thesis. University of Alberta Department of Civil Engineering, Structural Engineering.
- Ghodsi Nader Yoosef-, Kulak G. L. and Murray D. W. (1994). "Behaviour of Girth Welded Line-Pipe". University of Alberta Department of Civil Engineering, Structural Engineering. Report No. 23.
- Moħareb, M. E., Elwi, A. E., Kulak, G. L., and Murray, D. W. (1994). "Deformational Behaviour of Line Pipe". Structural Engineering Report No. 202, Department of Civil Engineering, University of Alberta, Edmonton, Alberta.
- Ju, G. T., and Kyriakides, S. (1992). "Instabilities in Cylindrical Shells under Bending – II. Predictions". International Journal of Solids Structures. Vol. 29, No.9, pp. 1143-1171.

Kyriakides, S. and Corona, E. (2007) "Mechanics of Offshore Pipelines: Volume 1 Buckling and Collapse". Elsevier. June 2007.

Walker, A. C. and Williams K. A. J. (1995). "Strain Based Design of Pipelines". Proceedings of OMAE, Vol.V, pp.345-350.

## **5. THESIS CONCLUSIONS AND RECOMMENDATIONS**

### **5.1. CONCLUSIONS**

The literature review has shown that the buckling behaviour of pipelines and cylindrical shells have been analyzed using a variety of tools. Analytical tools and physical experimentation were the only means of pipeline buckling research before computers and numerical techniques made it possible to study buckling with greater degree of complexity. While research currently favours numerical testing to development of analytical equations, physical testing is still required to calibrate numerical models and validate results.

The CSA Z662 strain based design equation does not make any allowance for girth weld imperfection whereas DNV OS-F101 accounts for the girth weld effect by using a design factor based on  $D/t$  ratio. With limited guidance on how to account for this form of imperfection, more research is needed to quantify the girth weld effect.

A finite element model has been developed and calibrated against physical data to investigate the buckling behaviour of girth welded pipes. The modeling procedure has demonstrated that the buckling characteristics and capacity of pipelines is highly dependant on diameter, thickness, internal pressure, applied axial load and misalignment imperfection as illustrated in the parametric study of these five parameters. The degree

of misalignment, in particular, was shown to reduce the moment and strain capacities by about 10% and 35% for moment and strain, respectively.

Further analysis of the parametric study results provided insight into the deformed shape of the buckled shape with respect to the design parameters as well as ovality characteristics of the pipelines. Diameter, thickness and internal pressure were found to be the dominant factors with respect to buckled wave forms and ovality. Decreasing  $D/t$  and increasing internal pressure were shown to increase in the wavelength and amplitude required to trigger buckling. In terms of ovality, it's measure typically increased with decreasing  $D/t$  ratio and pressure.

The total length of the pipe test section proved to be a critical factor in the buckling behaviour. It was found that end effects were predominant for pipe lengths of 3.5 diameters and highly influence the results as shown through the study of pipe sections having lengths of 5.5 and 10 diameters.

## **5.2. RECOMENDATIONS**

Knowledge obtain from this research has provided insight into the buckling behaviour of pipelines. The primary recommendation for further study of pipeline buckling based on this body of works is that length to diameter ratios for test sections should be as large as practical, for both numerical and physical tests. It was found that for some design cases studied, end effects assuredly influenced final results. This can be avoided with longer test sections. By studying longer pipe sections, the local moment-curvature may be

required as the global moment-curvature tends to be quite different compared to the local buckling moment.

Though the numerical model presented in this thesis have been calibrated to a series of test from the University of Alberta, Ghodsi et al. (1994) and Dorey (2001), it is uncertain whether or not the model can reliably predict full-scale behaviour of other pipeline system outside the scope of this study. A further validation study is required to enhance the confidence in the numerical results.

Given the nature of numerical analysis, the parametric study can readily be extended to include the effects of using other grade materials given the appropriate physical data. Material yield point, ultimate strength, anisotropy and the shape of the stress-strain curve are just some of the properties that could be investigated.

Even though the DNV OS-F101 strain equation is not intended for pipelines having a diameter to thickness ratio greater than 45, it was used in this study as a basis for comparison and shown to be very conservative when applied to pipelines with  $D/t$  equal to 90. Though thin walled pipelines are not usually used in offshore applications, a similar design equation may be tailored for onshore pipelines in buried configurations where large ground movements require strain based design. It is recommended that a strain based design equation be pursued in the future for thin walled pipelines.

## 6. REFERENCES

- Ades, C. S. (1957). "Bending Strength of Tubing in the Plastic Range". *Journal of Aeronautical Sciences*. pp. 605-610.
- Batterman, S. C. (1965). "Plastic Buckling of Axially Compressed Cylindrical Shells". *Journal of AIAA*. Vol. 3. pp. 316-325.
- Bouwkamp, J. G. and Stephen R. M. (1973). "Structural Behaviour of Large Diameter Pipe Under Combined Loading". *ASCE Transportation Engineering Journal*. TE3, Paper No. 9907.
- Bouwkamp, J. G. and Stephen R. M. (1974). "Full-Scale Studies on the Structural Behavior of Large Diameter Pipe Under Combined Loading." Report No. UC-SESM 74-1. Department of Civil Engineering, University of California, Berkeley, Jan. 1974.
- Brazier, L. G. (1927). "On the Flexure of Thin Cylindrical Shells and Other Thin Sections". *Proc., Royal Society, Series A*, Vol. 116, pp. 104-114.
- Bruschi, R., Monti, P., Bolzoni, G., and Tagliaferri, R. (1995). "Finite Element Method as Numerical Laboratory for Analysing Pipeline Response Under Internal Pressure, Axial Load, Bending Moment". *Proceedings of the 14<sup>th</sup> OMAE*, Vol.V, pp. 389-401.
- CSA Z662 (2003). "Oil and Gas Pipeline Systems". Canadian Standards Association.
- DNV OS-F101 (2000). "Submarine Pipeline Systems". Det Norske Veritas.
- Dorey, A. (2001). "Critical Buckling Strains in Energy Pipelines". Doctoral Thesis. University of Alberta Department of Civil Engineering, Structural Engineering.

- Dorey, A. B., Murray, D. W., and Cheng, J. J. R. (2006). "Initial Imperfection Models for Segments of Line Pipe". *Journal of Offshore Mechanics and Arctic Engineering*. Vol 128. pp. 322-329.
- Fatemi, A., Kenny, S., Cheragi, N., and Taheri, F. (2006). "Parametric Study on the Local Buckling Response of Pipelines Under Combined Loading Conditions". *Journal of Pipeline Integrity*. Vol 5. pp. 197-212.
- Ghodsi Nader Yoosef-, Kulak G. L. and Murray D. W. (1994). "Behaviour of Girth Welded Line-pipe". University of Alberta department of Civil Engineering, Structural Engineering. Report No. 23.
- Gresnigt, A. M. (1986). "Plastic Design of Buried Steel Pipelines in Settlement Areas". *Heron*, 31(4).
- Jirsa, J. O., Lee, F. H., Wilhoit, J. C., and Merwin, J. E. (1972). "Ovaling of Pipelines Under Pure Bending". *Proceedings of the Offshore Technology Conference*. Paper No. OTC1569.
- Johns, T. G. and Tamm, M. A. (1977). "Local Buckling of Cylindrical Columns Under Combined Loads". *Proceedings of the Offshore Technology Conference*. Paper No. OTC2952.
- Johns, T. G., Mesloh, R. E., Winegardner, R., and Sorenson, J. E. (1975). "Inelastic Buckling of Pipelines Under Combined Loads". *Proceedings of the Offshore Technology Conference*. Paper No. OTC2209.

- Ju, G. T., and Kyriakides, S. (1992). "Instabilities in Cylindrical Shells under Bending – II. Predictions". *International Journal of Solids Structures*. Vol. 29, No.9, pp. 1143-1171.
- Kyriakides, S. and Corona, E. (2007). "Mechanics of Offshore Pipelines: Volume 1 Buckling and Collapse". Elsevier. June 2007.
- Kyriakides, S., and Ju, G. T. (1992). "Bifurcation of Localization Instabilities in Cylindrical Shells Under Bending – I. Experiments". *International Journal of Solids Structures*. Vol. 29, No.9, pp. 1117-1142.
- Mohareb, M., Alexander, S. D. B, Kulak, G. L., and Murray, D. W. (1993). "Laboratory Testing of Line Pipe to Determine Deformational Behaviour". *Proceedings of the 12<sup>th</sup> OMAE*, Vol.V, pp.109-114.
- Mohareb, M., Kulak, G. L., Elwi, A., and Murray, D. W. (2001). "Testing and Analysis of Steel Pipe Segments". *Journal of Transportation Engineering*. Vol 127, No. 5, September/October 2001. pp. 408-417.
- Reddy, D. B. (1979). "An Experimental Study of the Plastic Buckling of Circular Cylinders in Pure Bending". *International Journal of Solid Structures*. Vol. 15, pp. 669-683.
- Row, D. G., Powell, G. H., and Morris, G. R. (1983). "Local Buckling Analysis of Pipelines". *Proceedings of the 2<sup>nd</sup> OMAE*. pp. 496-503. Houston, USA.
- Sherman, D. (1976). "Tests on Circular Steel Tubes in Bending". *ASCE Journal of Structural Division*. Vol. 102, ST11, pp. 2181-2195.

- Torselletti, E., Vitali, L., and Bruschi, R. (2005). "Bending Capacity of Girth-Welded Pipes". Proceedings of the 24<sup>th</sup> OMAE. Halkidiki, Greece.
- Vitali, L., Bruschi, R., Mork, K. J., Levold, E., and Verley, R. (1999). "Hotpipe Project: Capacity of Pipes Subject to Internal Pressure, Axial Force and Bending Moment". Proceedings of the 9<sup>th</sup> International Offshore and Polar Engineering Conference (ISOPE). pp. 22-32. Brest, France.
- Wilhoit, J. C., Jr. and Merwin, J. E. (1971). "The Effect of Axial Tension on Moment Carrying Capacity of Line Pipe Stressed Beyond the Elastic Limit". Proceedings of the Offshore Technology Conference. Paper No. OTC1355.
- Wilhoit, J. C., Jr. and Merwin, J. E. (1973). "Critical Plastic Buckling Parameters for Tubing in Bending Under Axial Tension". Proceedings of the Offshore Technology Conference. Paper No. OTC1874.
- Zimmerman, T. J. E., Stephens, M. J., DeGeer, D. D., and Chen, Q. (1995). "Compressive strain limits for buried pipelines." Proceedings of the 14<sup>th</sup> OMAE, Vol.V, pp. 365-378. Copenhagen, Denmark.
- Zimmerman, T., Timms, C., Xie, J., and Asante, J. (2004). "Buckling Resistance of Large Diameter Spiral Welded Linepipe." Proceedings of the International Pipeline Conference, IPC04-0364.

**APPENDIX A**

**Tabulated Results of Parametric Study**

Run Number	Outside Diameter (m)	Wall Thickness (m)	D/t (-)	Beta (-)	Pressure (Pa)	N (-)	Axial Force (N)	Imperfection (% tn)	Critical Moment (Nm)	Critical Curvature (-)	Normalized Strain	Normalized Moment	DNV Strain	DNV Moment
1	0.4064	0.01355	30	0.0	0.00E+00	-0.30	-2.42E+06	5.0	9.07E+05	4.84E-02	1.024	1.152	1.86E-02	7.87E+05
2	0.4064	0.01355	30	0.0	0.00E+00	-0.30	-2.42E+06	10.0	8.85E+05	3.84E-02	0.813	1.124	1.86E-02	7.87E+05
3	0.4064	0.01355	30	0.0	0.00E+00	-0.30	-2.42E+06	15.0	8.64E+05	3.30E-02	0.698	1.098	1.86E-02	7.87E+05
4	0.4064	0.01355	30	0.0	0.00E+00	-0.15	-1.21E+06	5.0	1.00E+06	6.01E-02	1.271	1.169	1.86E-02	8.55E+05
5	0.4064	0.01355	30	0.0	0.00E+00	-0.15	-1.21E+06	10.0	9.83E+05	4.69E-02	0.992	1.149	1.86E-02	8.55E+05
6	0.4064	0.01355	30	0.0	0.00E+00	-0.15	-1.21E+06	15.0	9.65E+05	3.98E-02	0.841	1.128	1.86E-02	8.55E+05
7	0.4064	0.01355	30	0.0	0.00E+00	0.00	0.00E+00	5.0	1.05E+06	7.63E-02	1.616	1.196	1.86E-02	8.78E+05
8	0.4064	0.01355	30	0.0	0.00E+00	0.00	0.00E+00	10.0	1.03E+06	6.08E-02	1.288	1.173	1.86E-02	8.78E+05
9	0.4064	0.01355	30	0.0	0.00E+00	0.00	0.00E+00	15.0	1.02E+06	5.16E-02	1.093	1.162	1.86E-02	8.78E+05
19	0.4064	0.01355	30	0.4	1.33E+07	-0.30	-4.03E+06	5.0	7.03E+05	7.16E-02	0.505	0.842	5.57E-02	8.35E+05
20	0.4064	0.01355	30	0.4	1.33E+07	-0.30	-4.03E+06	10.0	6.85E+05	5.62E-02	0.397	0.820	5.57E-02	8.35E+05
21	0.4064	0.01355	30	0.4	1.33E+07	-0.30	-4.03E+06	15.0	6.66E+05	4.63E-02	0.326	0.798	5.57E-02	8.35E+05
22	0.4064	0.01355	30	0.4	1.33E+07	-0.15	-2.82E+06	5.0	8.57E+05	8.43E-02	0.595	0.929	5.57E-02	9.23E+05
23	0.4064	0.01355	30	0.4	1.33E+07	-0.15	-2.82E+06	10.0	8.40E+05	6.61E-02	0.466	0.910	5.57E-02	9.23E+05
24	0.4064	0.01355	30	0.4	1.33E+07	-0.15	-2.82E+06	15.0	8.24E+05	5.50E-02	0.388	0.893	5.57E-02	9.23E+05
25	0.4064	0.01355	30	0.4	1.33E+07	0.00	-1.61E+06	5.0	9.68E+05	1.05E-01	0.744	1.017	5.57E-02	9.52E+05
26	0.4064	0.01355	30	0.4	1.33E+07	0.00	-1.61E+06	10.0	9.51E+05	8.12E-02	0.573	0.999	5.57E-02	9.52E+05
27	0.4064	0.01355	30	0.4	1.33E+07	0.00	-1.61E+06	15.0	9.38E+05	6.83E-02	0.482	0.985	5.57E-02	9.52E+05
37	0.4064	0.01355	30	0.8	2.66E+07	-0.30	-5.64E+06	5.0	2.50E+05	1.06E-01	0.448	0.496	9.28E-02	5.04E+05
38	0.4064	0.01355	30	0.8	2.66E+07	-0.30	-5.64E+06	10.0	2.43E+05	9.75E-02	0.413	0.482	9.28E-02	5.04E+05
39	0.4064	0.01355	30	0.8	2.66E+07	-0.30	-5.64E+06	15.0	2.34E+05	8.85E-02	0.375	0.465	9.28E-02	5.04E+05
40	0.4064	0.01355	30	0.8	2.66E+07	-0.15	-4.43E+06	5.0	4.69E+05	1.24E-01	0.524	0.715	9.28E-02	6.56E+05
41	0.4064	0.01355	30	0.8	2.66E+07	-0.15	-4.43E+06	10.0	4.61E+05	1.11E-01	0.472	0.703	9.28E-02	6.56E+05
42	0.4064	0.01355	30	0.8	2.66E+07	-0.15	-4.43E+06	15.0	4.54E+05	1.03E-01	0.434	0.692	9.28E-02	6.56E+05
43	0.4064	0.01355	30	0.8	2.66E+07	0.00	-3.22E+06	5.0	6.58E+05	1.53E-01	0.648	0.931	9.28E-02	7.07E+05
44	0.4064	0.01355	30	0.8	2.66E+07	0.00	-3.22E+06	10.0	6.48E+05	1.33E-01	0.563	0.917	9.28E-02	7.07E+05
45	0.4064	0.01355	30	0.8	2.66E+07	0.00	-3.22E+06	15.0	6.41E+05	1.22E-01	0.517	0.907	9.28E-02	7.07E+05

Run Number	Outside Diameter (m)	Wall Thickness (m)	D/t (-)	Beta (-)	Pressure (Pa)	N (-)	Axial Force (N)	Imperfection (% tn)	Critical Moment (Nm)	Critical Curvature (-)	Normalized Strain	Normalized Moment	DNV Strain	DNV Moment
10	0.6096	0.02032	30	0.0	0.00E+00	-0.30	-5.44E+06	5.0	3.07E+06	3.46E-02	1.098	1.156	1.86E-02	2.66E+06
11	0.6096	0.02032	30	0.0	0.00E+00	-0.30	-5.44E+06	10.0	3.00E+06	2.71E-02	0.860	1.129	1.86E-02	2.66E+06
12	0.6096	0.02032	30	0.0	0.00E+00	-0.30	-5.44E+06	14.8	2.93E+06	2.32E-02	0.736	1.103	1.86E-02	2.66E+06
13	0.6096	0.02032	30	0.0	0.00E+00	-0.15	-2.72E+06	5.0	3.39E+06	4.20E-02	1.334	1.174	1.86E-02	2.89E+06
14	0.6096	0.02032	30	0.0	0.00E+00	-0.15	-2.72E+06	10.0	3.33E+06	3.30E-02	1.048	1.154	1.86E-02	2.89E+06
15	0.6096	0.02032	30	0.0	0.00E+00	-0.15	-2.72E+06	14.8	3.27E+06	2.80E-02	0.888	1.133	1.86E-02	2.89E+06
16	0.6096	0.02032	30	0.0	0.00E+00	0.00	0.00E+00	5.0	3.55E+06	5.45E-02	1.730	1.198	1.86E-02	2.96E+06
17	0.6096	0.02032	30	0.0	0.00E+00	0.00	0.00E+00	10.0	3.50E+06	4.29E-02	1.362	1.181	1.86E-02	2.96E+06
18	0.6096	0.02032	30	0.0	0.00E+00	0.00	0.00E+00	14.8	3.45E+06	3.64E-02	1.155	1.164	1.86E-02	2.96E+06
28	0.6096	0.02032	30	0.4	1.33E+07	-0.30	-9.07E+06	5.0	2.39E+06	5.09E-02	0.539	0.848	5.57E-02	2.82E+06
29	0.6096	0.02032	30	0.4	1.33E+07	-0.30	-9.07E+06	10.0	2.32E+06	3.97E-02	0.420	0.823	5.57E-02	2.82E+06
30	0.6096	0.02032	30	0.4	1.33E+07	-0.30	-9.07E+06	14.8	2.27E+06	3.38E-02	0.358	0.806	5.57E-02	2.82E+06
31	0.6096	0.02032	30	0.4	1.33E+07	-0.15	-6.35E+06	5.0	2.90E+06	5.97E-02	0.632	0.931	5.57E-02	3.11E+06
32	0.6096	0.02032	30	0.4	1.33E+07	-0.15	-6.35E+06	10.0	2.84E+06	4.63E-02	0.490	0.912	5.57E-02	3.11E+06
33	0.6096	0.02032	30	0.4	1.33E+07	-0.15	-6.35E+06	14.8	2.80E+06	3.92E-02	0.415	0.899	5.57E-02	3.11E+06
34	0.6096	0.02032	30	0.4	1.33E+07	0.00	-3.63E+06	5.0	3.28E+06	7.55E-02	0.799	1.021	5.57E-02	3.21E+06
35	0.6096	0.02032	30	0.4	1.33E+07	0.00	-3.63E+06	10.0	3.22E+06	5.77E-02	0.611	1.002	5.57E-02	3.21E+06
36	0.6096	0.02032	30	0.4	1.33E+07	0.00	-3.63E+06	14.8	3.18E+06	4.87E-02	0.515	0.989	5.57E-02	3.21E+06
46	0.6096	0.02032	30	0.8	2.66E+07	-0.30	-1.27E+07	5.0	8.73E+05	7.73E-02	0.491	0.514	9.28E-02	1.70E+06
47	0.6096	0.02032	30	0.8	2.66E+07	-0.30	-1.27E+07	10.0	8.40E+05	6.85E-02	0.435	0.494	9.28E-02	1.70E+06
48	0.6096	0.02032	30	0.8	2.66E+07	-0.30	-1.27E+07	14.8	8.09E+05	6.23E-02	0.396	0.476	9.28E-02	1.70E+06
49	0.6096	0.02032	30	0.8	2.66E+07	-0.15	-9.97E+06	5.0	1.61E+06	8.79E-02	0.558	0.727	9.28E-02	2.21E+06
50	0.6096	0.02032	30	0.8	2.66E+07	-0.15	-9.97E+06	10.0	1.58E+06	7.83E-02	0.497	0.714	9.28E-02	2.21E+06
51	0.6096	0.02032	30	0.8	2.66E+07	-0.15	-9.97E+06	14.8	1.55E+06	7.18E-02	0.456	0.700	9.28E-02	2.21E+06
52	0.6096	0.02032	30	0.8	2.66E+07	0.00	-7.25E+06	5.0	2.23E+06	1.05E-01	0.666	0.935	9.28E-02	2.39E+06
53	0.6096	0.02032	30	0.8	2.66E+07	0.00	-7.25E+06	10.0	2.20E+06	9.31E-02	0.591	0.922	9.28E-02	2.39E+06
54	0.6096	0.02032	30	0.8	2.66E+07	0.00	-7.25E+06	14.8	2.17E+06	8.45E-02	0.536	0.910	9.28E-02	2.39E+06

Run Number	Outside Diameter (m)	Wall Thickness (m)	D/t (-)	Beta (-)	Pressure (Pa)	N (-)	Axial Force (N)	Imperfection (% tn)	Critical Moment (Nm)	Critical Curvature (-)	Normalized Strain	Normalized Moment	DNV Strain	DNV Moment
1	0.9144	0.03048	30	0.0	0.00E+00	-0.30	-1.22E+07	5.0	1.04E+07	2.36E-02	1.123	1.160	1.86E-02	8.97E+06
2	0.9144	0.03048	30	0.0	0.00E+00	-0.30	-1.22E+07	9.8	1.01E+07	1.86E-02	0.885	1.126	1.86E-02	8.97E+06
3	0.9144	0.03048	30	0.0	0.00E+00	-0.30	-1.22E+07	9.8	1.01E+07	1.86E-02	0.885	1.126	1.86E-02	8.97E+06
4	0.9144	0.03048	30	0.0	0.00E+00	-0.15	-6.12E+06	5.0	1.14E+07	2.81E-02	1.337	1.170	1.86E-02	9.74E+06
5	0.9144	0.03048	30	0.0	0.00E+00	-0.15	-6.12E+06	9.8	1.12E+07	2.22E-02	1.057	1.150	1.86E-02	9.74E+06
6	0.9144	0.03048	30	0.0	0.00E+00	-0.15	-6.12E+06	9.8	1.12E+07	2.22E-02	1.057	1.150	1.86E-02	9.74E+06
7	0.9144	0.03048	30	0.0	0.00E+00	0.00	0.00E+00	5.0	1.20E+07	3.67E-02	1.749	1.200	1.86E-02	1.00E+07
8	0.9144	0.03048	30	0.0	0.00E+00	0.00	0.00E+00	9.8	1.18E+07	2.91E-02	1.386	1.180	1.86E-02	1.00E+07
9	0.9144	0.03048	30	0.0	0.00E+00	0.00	0.00E+00	9.8	1.18E+07	2.91E-02	1.386	1.180	1.86E-02	1.00E+07
10	0.9144	0.03048	30	0.4	1.33E+07	-0.30	-2.04E+07	5.0	8.08E+06	3.41E-02	0.542	0.850	5.57E-02	9.51E+06
11	0.9144	0.03048	30	0.4	1.33E+07	-0.30	-2.04E+07	9.8	7.85E+06	2.65E-02	0.421	0.825	5.57E-02	9.51E+06
12	0.9144	0.03048	30	0.4	1.33E+07	-0.30	-2.04E+07	9.8	7.85E+06	2.65E-02	0.421	0.825	5.57E-02	9.51E+06
13	0.9144	0.03048	30	0.4	1.33E+07	-0.15	-1.43E+07	5.0	9.80E+06	3.97E-02	0.630	0.932	5.57E-02	1.05E+07
14	0.9144	0.03048	30	0.4	1.33E+07	-0.15	-1.43E+07	9.8	9.61E+06	3.11E-02	0.494	0.914	5.57E-02	1.05E+07
15	0.9144	0.03048	30	0.4	1.33E+07	-0.15	-1.43E+07	9.8	9.61E+06	3.11E-02	0.494	0.914	5.57E-02	1.05E+07
16	0.9144	0.03048	30	0.4	1.33E+07	0.00	-8.16E+06	5.0	1.11E+07	5.10E-02	0.810	1.023	5.57E-02	1.08E+07
17	0.9144	0.03048	30	0.4	1.33E+07	0.00	-8.16E+06	9.8	1.09E+07	3.91E-02	0.620	1.005	5.57E-02	1.08E+07
18	0.9144	0.03048	30	0.4	1.33E+07	0.00	-8.16E+06	9.8	1.09E+07	3.91E-02	0.620	1.005	5.57E-02	1.08E+07
19	0.9144	0.03048	30	0.8	2.66E+07	-0.30	-2.86E+07	5.0	3.02E+06	5.37E-02	0.512	0.526	9.28E-02	5.74E+06
20	0.9144	0.03048	30	0.8	2.66E+07	-0.30	-2.86E+07	9.8	2.88E+06	4.70E-02	0.448	0.502	9.28E-02	5.74E+06
21	0.9144	0.03048	30	0.8	2.66E+07	-0.30	-2.86E+07	9.8	2.88E+06	4.70E-02	0.448	0.502	9.28E-02	5.74E+06
22	0.9144	0.03048	30	0.8	2.66E+07	-0.15	-2.24E+07	5.0	5.51E+06	6.20E-02	0.591	0.737	9.28E-02	7.47E+06
23	0.9144	0.03048	30	0.8	2.66E+07	-0.15	-2.24E+07	9.8	5.37E+06	5.40E-02	0.514	0.719	9.28E-02	7.47E+06
24	0.9144	0.03048	30	0.8	2.66E+07	-0.15	-2.24E+07	9.8	5.37E+06	5.40E-02	0.514	0.719	9.28E-02	7.47E+06
25	0.9144	0.03048	30	0.8	2.66E+07	0.00	-1.63E+07	5.0	7.64E+06	7.52E-02	0.716	0.949	9.28E-02	8.05E+06
26	0.9144	0.03048	30	0.8	2.66E+07	0.00	-1.63E+07	9.8	7.47E+06	6.38E-02	0.608	0.928	9.28E-02	8.05E+06
27	0.9144	0.03048	30	0.8	2.66E+07	0.00	-1.63E+07	9.8	7.47E+06	6.38E-02	0.608	0.928	9.28E-02	8.05E+06

Run Number	Outside Diameter (m)	Wall Thickness (m)	D/t (-)	Beta (-)	Pressure (Pa)	N (-)	Axial Force (N)	Imperfection (% tn)	Critical Moment (Nm)	Critical Curvature (-)	Normalized Strain	Normalized Moment	DNV Strain	DNV Moment
55	0.4064	0.00677	60	0.0	0.00E+00	-0.30	-1.23E+06	5.0	4.17E+05	1.97E-02	2.227	1.024	3.54E-03	4.07E+05
56	0.4064	0.00677	60	0.0	0.00E+00	-0.30	-1.23E+06	10.0	3.94E+05	1.67E-02	1.887	0.967	3.54E-03	4.07E+05
57	0.4064	0.00677	60	0.0	0.00E+00	-0.30	-1.23E+06	15.0	3.76E+05	1.52E-02	1.721	0.923	3.54E-03	4.07E+05
58	0.4064	0.00677	60	0.0	0.00E+00	-0.15	-6.15E+05	5.0	4.71E+05	2.21E-02	2.499	1.064	3.54E-03	4.43E+05
59	0.4064	0.00677	60	0.0	0.00E+00	-0.15	-6.15E+05	10.0	4.58E+05	1.98E-02	2.238	1.035	3.54E-03	4.43E+05
60	0.4064	0.00677	60	0.0	0.00E+00	-0.15	-6.15E+05	15.0	4.42E+05	1.76E-02	1.987	0.999	3.54E-03	4.43E+05
61	0.4064	0.00677	60	0.0	0.00E+00	0.00	0.00E+00	5.0	5.05E+05	2.81E-02	3.180	1.112	3.54E-03	4.54E+05
62	0.4064	0.00677	60	0.0	0.00E+00	0.00	0.00E+00	10.0	4.93E+05	2.43E-02	2.750	1.085	3.54E-03	4.54E+05
63	0.4064	0.00677	60	0.0	0.00E+00	0.00	0.00E+00	15.0	4.83E+05	2.18E-02	2.467	1.063	3.54E-03	4.54E+05
73	0.4064	0.00677	60	0.4	6.54E+06	-0.30	-2.05E+06	5.0	3.17E+05	2.54E-02	0.957	0.734	1.06E-02	4.32E+05
74	0.4064	0.00677	60	0.4	6.54E+06	-0.30	-2.05E+06	10.0	2.97E+05	2.01E-02	0.756	0.688	1.06E-02	4.32E+05
75	0.4064	0.00677	60	0.4	6.54E+06	-0.30	-2.05E+06	15.0	2.88E+05	1.83E-02	0.689	0.667	1.06E-02	4.32E+05
76	0.4064	0.00677	60	0.4	6.54E+06	-0.15	-1.43E+06	5.0	4.02E+05	2.87E-02	1.080	0.842	1.06E-02	4.78E+05
77	0.4064	0.00677	60	0.4	6.54E+06	-0.15	-1.43E+06	10.0	3.87E+05	2.38E-02	0.895	0.810	1.06E-02	4.78E+05
78	0.4064	0.00677	60	0.4	6.54E+06	-0.15	-1.43E+06	15.0	3.69E+05	2.00E-02	0.755	0.773	1.06E-02	4.78E+05
79	0.4064	0.00677	60	0.4	6.54E+06	0.00	-8.20E+05	5.0	4.64E+05	3.40E-02	1.283	0.942	1.06E-02	4.93E+05
80	0.4064	0.00677	60	0.4	6.54E+06	0.00	-8.20E+05	10.0	4.52E+05	2.86E-02	1.076	0.917	1.06E-02	4.93E+05
81	0.4064	0.00677	60	0.4	6.54E+06	0.00	-8.20E+05	15.0	4.39E+05	2.41E-02	0.909	0.891	1.06E-02	4.93E+05
91	0.4064	0.00677	60	0.8	1.31E+07	-0.30	-2.87E+06	5.0	9.04E+04	3.83E-02	0.865	0.347	1.77E-02	2.61E+05
92	0.4064	0.00677	60	0.8	1.31E+07	-0.30	-2.87E+06	10.0	8.84E+04	3.67E-02	0.829	0.339	1.77E-02	2.61E+05
93	0.4064	0.00677	60	0.8	1.31E+07	-0.30	-2.87E+06	15.0	8.23E+04	2.86E-02	0.647	0.316	1.77E-02	2.61E+05
94	0.4064	0.00677	60	0.8	1.31E+07	-0.15	-2.25E+06	5.0	2.01E+05	4.60E-02	1.039	0.592	1.77E-02	3.39E+05
95	0.4064	0.00677	60	0.8	1.31E+07	-0.15	-2.25E+06	10.0	1.99E+05	4.47E-02	1.010	0.586	1.77E-02	3.39E+05
96	0.4064	0.00677	60	0.8	1.31E+07	-0.15	-2.25E+06	15.0	1.90E+05	3.63E-02	0.820	0.560	1.77E-02	3.39E+05
97	0.4064	0.00677	60	0.8	1.31E+07	0.00	-1.64E+06	5.0	3.01E+05	5.44E-02	1.229	0.823	1.77E-02	3.66E+05
98	0.4064	0.00677	60	0.8	1.31E+07	0.00	-1.64E+06	10.0	2.97E+05	4.83E-02	1.092	0.812	1.77E-02	3.66E+05
99	0.4064	0.00677	60	0.8	1.31E+07	0.00	-1.64E+06	15.0	2.91E+05	4.23E-02	0.955	0.796	1.77E-02	3.66E+05

Run Number	Outside Diameter (m)	Wall Thickness (m)	D/t (-)	Beta (-)	Pressure (Pa)	N (-)	Axial Force (N)	Imperfection (% tn)	Critical Moment (Nm)	Critical Curvature (-)	Normalized Strain	Normalized Moment	DNV Strain	DNV Moment
64	0.6096	0.01016	60	0.0	0.00E+00	-0.30	-2.77E+06	5.0	1.40E+06	1.34E-02	2.267	1.019	3.54E-03	1.37E+06
65	0.6096	0.01016	60	0.0	0.00E+00	-0.30	-2.77E+06	10.0	1.32E+06	1.12E-02	1.905	0.960	3.54E-03	1.37E+06
66	0.6096	0.01016	60	0.0	0.00E+00	-0.30	-2.77E+06	15.0	1.20E+06	9.64E-03	1.634	0.873	3.54E-03	1.37E+06
67	0.6096	0.01016	60	0.0	0.00E+00	-0.15	-1.38E+06	5.0	1.60E+06	1.56E-02	2.651	1.071	3.54E-03	1.49E+06
68	0.6096	0.01016	60	0.0	0.00E+00	-0.15	-1.38E+06	10.0	1.53E+06	1.32E-02	2.236	1.024	3.54E-03	1.49E+06
69	0.6096	0.01016	60	0.0	0.00E+00	-0.15	-1.38E+06	15.0	1.48E+06	1.19E-02	2.020	0.991	3.54E-03	1.49E+06
70	0.6096	0.01016	60	0.0	0.00E+00	0.00	0.00E+00	5.0	1.70E+06	1.92E-02	3.250	1.109	3.54E-03	1.53E+06
71	0.6096	0.01016	60	0.0	0.00E+00	0.00	0.00E+00	10.0	1.66E+06	1.65E-02	2.799	1.083	3.54E-03	1.53E+06
72	0.6096	0.01016	60	0.0	0.00E+00	0.00	0.00E+00	15.0	1.62E+06	1.47E-02	2.491	1.057	3.54E-03	1.53E+06
82	0.6096	0.01016	60	0.4	6.54E+06	-0.30	-4.61E+06	5.0	1.06E+06	1.70E-02	0.960	0.727	1.06E-02	1.46E+06
83	0.6096	0.01016	60	0.4	6.54E+06	-0.30	-4.61E+06	10.0	1.01E+06	1.41E-02	0.796	0.693	1.06E-02	1.46E+06
84	0.6096	0.01016	60	0.4	6.54E+06	-0.30	-4.61E+06	15.0	9.63E+05	1.23E-02	0.698	0.661	1.06E-02	1.46E+06
85	0.6096	0.01016	60	0.4	6.54E+06	-0.15	-3.23E+06	5.0	1.35E+06	1.95E-02	1.104	0.838	1.06E-02	1.61E+06
86	0.6096	0.01016	60	0.4	6.54E+06	-0.15	-3.23E+06	10.0	1.29E+06	1.55E-02	0.876	0.800	1.06E-02	1.61E+06
87	0.6096	0.01016	60	0.4	6.54E+06	-0.15	-3.23E+06	15.0	1.26E+06	1.43E-02	0.807	0.782	1.06E-02	1.61E+06
88	0.6096	0.01016	60	0.4	6.54E+06	0.00	-1.84E+06	5.0	1.56E+06	2.36E-02	1.333	0.938	1.06E-02	1.66E+06
89	0.6096	0.01016	60	0.4	6.54E+06	0.00	-1.84E+06	10.0	1.52E+06	1.92E-02	1.084	0.914	1.06E-02	1.66E+06
90	0.6096	0.01016	60	0.4	6.54E+06	0.00	-1.84E+06	15.0	1.48E+06	1.70E-02	0.960	0.890	1.06E-02	1.66E+06
100	0.6096	0.01016	60	0.8	1.31E+07	-0.30	-6.46E+06	5.0	3.07E+05	2.67E-02	0.904	0.349	1.77E-02	8.79E+05
101	0.6096	0.01016	60	0.8	1.31E+07	-0.30	-6.46E+06	10.0	2.98E+05	2.46E-02	0.836	0.339	1.77E-02	8.79E+05
102	0.6096	0.01016	60	0.8	1.31E+07	-0.30	-6.46E+06	15.0	2.78E+05	2.07E-02	0.701	0.316	1.77E-02	8.79E+05
103	0.6096	0.01016	60	0.8	1.31E+07	-0.15	-5.07E+06	5.0	6.89E+05	3.38E-02	1.148	0.601	1.77E-02	1.15E+06
104	0.6096	0.01016	60	0.8	1.31E+07	-0.15	-5.07E+06	10.0	6.75E+05	3.05E-02	1.035	0.589	1.77E-02	1.15E+06
105	0.6096	0.01016	60	0.8	1.31E+07	-0.15	-5.07E+06	15.0	6.48E+05	2.59E-02	0.877	0.566	1.77E-02	1.15E+06
106	0.6096	0.01016	60	0.8	1.31E+07	0.00	-3.69E+06	5.0	1.02E+06	3.95E-02	1.338	0.826	1.77E-02	1.23E+06
107	0.6096	0.01016	60	0.8	1.31E+07	0.00	-3.69E+06	10.0	1.00E+06	3.39E-02	1.151	0.810	1.77E-02	1.23E+06
108	0.6096	0.01016	60	0.8	1.31E+07	0.00	-3.69E+06	15.0	9.86E+05	3.05E-02	1.034	0.799	1.77E-02	1.23E+06

Run Number	Outside Diameter (m)	Wall Thickness (m)	D/t (-)	Beta (-)	Pressure (Pa)	N (-)	Axial Force (N)	Imperfection (% tn)	Critical Moment (Nm)	Critical Curvature (-)	Normalized Strain	Normalized Moment	DNV Strain	DNV Moment
28	0.9144	0.01524	60	0.0	0.00E+00	-0.30	-6.23E+06	5.0	4.67E+06	8.98E-03	2.283	1.007	3.54E-03	4.64E+06
29	0.9144	0.01524	60	0.0	0.00E+00	-0.30	-6.23E+06	10.0	4.36E+06	7.42E-03	1.887	0.940	3.54E-03	4.64E+06
30	0.9144	0.01524	60	0.0	0.00E+00	-0.30	-6.23E+06	15.0	4.09E+06	6.61E-03	1.682	0.882	3.54E-03	4.64E+06
31	0.9144	0.01524	60	0.0	0.00E+00	-0.15	-3.11E+06	5.0	5.33E+06	1.05E-02	2.668	1.057	3.54E-03	5.04E+06
32	0.9144	0.01524	60	0.0	0.00E+00	-0.15	-3.11E+06	10.0	5.12E+06	8.91E-03	2.267	1.016	3.54E-03	5.04E+06
33	0.9144	0.01524	60	0.0	0.00E+00	-0.15	-3.11E+06	15.0	4.93E+06	7.92E-03	2.014	0.978	3.54E-03	5.04E+06
34	0.9144	0.01524	60	0.0	0.00E+00	0.00	0.00E+00	5.0	5.68E+06	1.30E-02	3.304	1.098	3.54E-03	5.18E+06
35	0.9144	0.01524	60	0.0	0.00E+00	0.00	0.00E+00	10.0	5.52E+06	1.09E-02	2.771	1.067	3.54E-03	5.18E+06
36	0.9144	0.01524	60	0.0	0.00E+00	0.00	0.00E+00	15.0	5.38E+06	9.78E-03	2.486	1.040	3.54E-03	5.18E+06
37	0.9144	0.01524	60	0.4	6.54E+06	-0.30	-1.04E+07	5.0	3.50E+06	1.11E-02	0.943	0.711	1.06E-02	4.92E+06
38	0.9144	0.01524	60	0.4	6.54E+06	-0.30	-1.04E+07	10.0	3.35E+06	9.64E-03	0.817	0.681	1.06E-02	4.92E+06
39	0.9144	0.01524	60	0.4	6.54E+06	-0.30	-1.04E+07	15.0	3.14E+06	7.96E-03	0.675	0.638	1.06E-02	4.92E+06
40	0.9144	0.01524	60	0.4	6.54E+06	-0.15	-7.26E+06	5.0	4.50E+06	1.32E-02	1.116	0.827	1.06E-02	5.44E+06
41	0.9144	0.01524	60	0.4	6.54E+06	-0.15	-7.26E+06	10.0	4.34E+06	1.10E-02	0.935	0.798	1.06E-02	5.44E+06
42	0.9144	0.01524	60	0.4	6.54E+06	-0.15	-7.26E+06	15.0	4.20E+06	9.71E-03	0.823	0.772	1.06E-02	5.44E+06
43	0.9144	0.01524	60	0.4	6.54E+06	0.00	-4.15E+06	5.0	5.16E+06	1.46E-02	1.236	0.919	1.06E-02	5.61E+06
44	0.9144	0.01524	60	0.4	6.54E+06	0.00	-4.15E+06	10.0	5.08E+06	1.30E-02	1.104	0.905	1.06E-02	5.61E+06
45	0.9144	0.01524	60	0.4	6.54E+06	0.00	-4.15E+06	15.0	4.94E+06	1.13E-02	0.956	0.880	1.06E-02	5.61E+06
46	0.9144	0.01524	60	0.8	1.31E+07	-0.30	-1.45E+07	5.0	9.92E+05	1.97E-02	1.003	0.334	1.77E-02	2.97E+06
47	0.9144	0.01524	60	0.8	1.31E+07	-0.30	-1.45E+07	10.0	9.23E+05	1.57E-02	0.799	0.311	1.77E-02	2.97E+06
48	0.9144	0.01524	60	0.8	1.31E+07	-0.30	-1.45E+07	15.0	8.60E+05	1.36E-02	0.694	0.290	1.77E-02	2.97E+06
49	0.9144	0.01524	60	0.8	1.31E+07	-0.15	-1.14E+07	5.0	2.27E+06	2.44E-02	1.241	0.587	1.77E-02	3.87E+06
50	0.9144	0.01524	60	0.8	1.31E+07	-0.15	-1.14E+07	10.0	2.17E+06	1.94E-02	0.987	0.561	1.77E-02	3.87E+06
51	0.9144	0.01524	60	0.8	1.31E+07	-0.15	-1.14E+07	15.0	2.10E+06	1.74E-02	0.883	0.543	1.77E-02	3.87E+06
52	0.9144	0.01524	60	0.8	1.31E+07	0.00	-8.30E+06	5.0	3.41E+06	2.86E-02	1.454	0.819	1.77E-02	4.17E+06
53	0.9144	0.01524	60	0.8	1.31E+07	0.00	-8.30E+06	10.0	3.32E+06	2.31E-02	1.175	0.797	1.77E-02	4.17E+06
54	0.9144	0.01524	60	0.8	1.31E+07	0.00	-8.30E+06	15.0	3.24E+06	2.01E-02	1.022	0.778	1.77E-02	4.17E+06

Run Number	Outside Diameter (m)	Wall Thickness (m)	D/t (-)	Beta (-)	Pressure (Pa)	N (-)	Axial Force (N)	Imperfection (% tn)	Critical Moment (Nm)	Critical Curvature (-)	Normalized Strain	Normalized Moment	DNV Strain	DNV Moment
109	0.4064	0.00452	90	0.0	0.00E+00	-0.30	-8.24E+05	5.0	2.48E+05	1.37E-02	9.336	0.903	5.89E-04	2.75E+05
110	0.4064	0.00452	90	0.0	0.00E+00	-0.30	-8.24E+05	10.0	2.33E+05	1.20E-02	8.189	0.848	5.89E-04	2.75E+05
111	0.4064	0.00452	90	0.0	0.00E+00	-0.30	-8.24E+05	15.0	2.20E+05	1.10E-02	7.482	0.801	5.89E-04	2.75E+05
112	0.4064	0.00452	90	0.0	0.00E+00	-0.15	-4.12E+05	5.0	2.91E+05	1.56E-02	10.614	0.975	5.89E-04	2.98E+05
113	0.4064	0.00452	90	0.0	0.00E+00	-0.15	-4.12E+05	10.0	2.79E+05	1.41E-02	9.587	0.935	5.89E-04	2.98E+05
114	0.4064	0.00452	90	0.0	0.00E+00	-0.15	-4.12E+05	15.0	2.68E+05	1.30E-02	8.844	0.898	5.89E-04	2.98E+05
115	0.4064	0.00452	90	0.0	0.00E+00	0.00	0.00E+00	5.0	3.20E+05	1.96E-02	13.349	1.045	5.89E-04	3.06E+05
116	0.4064	0.00452	90	0.0	0.00E+00	0.00	0.00E+00	10.0	3.07E+05	1.66E-02	11.331	1.002	5.89E-04	3.06E+05
117	0.4064	0.00452	90	0.0	0.00E+00	0.00	0.00E+00	15.0	2.99E+05	1.54E-02	10.471	0.976	5.89E-04	3.06E+05
127	0.4064	0.00452	90	0.4	4.33E+06	-0.30	-1.37E+06	5.0	1.83E+05	1.51E-02	3.423	0.628	1.77E-03	2.91E+05
128	0.4064	0.00452	90	0.4	4.33E+06	-0.30	-1.37E+06	10.0	1.73E+05	1.30E-02	2.947	0.594	1.77E-03	2.91E+05
129	0.4064	0.00452	90	0.4	4.33E+06	-0.30	-1.37E+06	15.0	1.62E+05	1.11E-02	2.525	0.556	1.77E-03	2.91E+05
130	0.4064	0.00452	90	0.4	4.33E+06	-0.15	-9.62E+05	5.0	2.39E+05	1.72E-02	3.919	0.742	1.77E-03	3.22E+05
131	0.4064	0.00452	90	0.4	4.33E+06	-0.15	-9.62E+05	10.0	2.27E+05	1.49E-02	3.391	0.705	1.77E-03	3.22E+05
132	0.4064	0.00452	90	0.4	4.33E+06	-0.15	-9.62E+05	15.0	2.19E+05	1.37E-02	3.109	0.680	1.77E-03	3.22E+05
133	0.4064	0.00452	90	0.4	4.33E+06	0.00	-5.50E+05	5.0	2.87E+05	2.07E-02	4.699	0.864	1.77E-03	3.32E+05
134	0.4064	0.00452	90	0.4	4.33E+06	0.00	-5.50E+05	10.0	2.77E+05	1.78E-02	4.039	0.834	1.77E-03	3.32E+05
135	0.4064	0.00452	90	0.4	4.33E+06	0.00	-5.50E+05	15.0	2.67E+05	1.59E-02	3.610	0.804	1.77E-03	3.32E+05
145	0.4064	0.00452	90	0.8	8.67E+06	-0.30	-1.92E+06	5.0	3.74E+04	1.68E-02	2.287	0.213	2.95E-03	1.76E+05
146	0.4064	0.00452	90	0.8	8.67E+06	-0.30	-1.92E+06	10.0	3.87E+04	1.79E-02	2.440	0.220	2.95E-03	1.76E+05
147	0.4064	0.00452	90	0.8	8.67E+06	-0.30	-1.92E+06	15.0	3.46E+04	1.39E-02	1.892	0.197	2.95E-03	1.76E+05
148	0.4064	0.00452	90	0.8	8.67E+06	-0.15	-1.51E+06	5.0	1.10E+05	2.49E-02	3.395	0.481	2.95E-03	2.29E+05
149	0.4064	0.00452	90	0.8	8.67E+06	-0.15	-1.51E+06	10.0	1.09E+05	2.41E-02	3.285	0.476	2.95E-03	2.29E+05
150	0.4064	0.00452	90	0.8	8.67E+06	-0.15	-1.51E+06	15.0	1.05E+05	2.10E-02	2.864	0.459	2.95E-03	2.29E+05
151	0.4064	0.00452	90	0.8	8.67E+06	0.00	-1.10E+06	5.0	1.78E+05	3.08E-02	4.201	0.722	2.95E-03	2.47E+05
152	0.4064	0.00452	90	0.8	8.67E+06	0.00	-1.10E+06	10.0	1.76E+05	2.75E-02	3.748	0.714	2.95E-03	2.47E+05
153	0.4064	0.00452	90	0.8	8.67E+06	0.00	-1.10E+06	15.0	1.73E+05	2.58E-02	3.524	0.702	2.95E-03	2.47E+05

Run Number	Outside Diameter (m)	Wall Thickness (m)	D/t (-)	Beta (-)	Pressure (Pa)	N (-)	Axial Force (N)	Imperfection (% tn)	Critical Moment (Nm)	Critical Curvature (-)	Normalized Strain	Normalized Moment	DNV Strain	DNV Moment
118	0.6096	0.00677	90	0.0	0.00E+00	-0.30	-1.85E+06	5.0	8.35E+05	9.22E-03	9.431	0.901	5.89E-04	9.27E+05
119	0.6096	0.00677	90	0.0	0.00E+00	-0.30	-1.85E+06	10.0	7.82E+05	8.10E-03	8.289	0.844	5.89E-04	9.27E+05
120	0.6096	0.00677	90	0.0	0.00E+00	-0.30	-1.85E+06	15.0	7.18E+05	6.96E-03	7.124	0.775	5.89E-04	9.27E+05
121	0.6096	0.00677	90	0.0	0.00E+00	-0.15	-9.27E+05	5.0	9.75E+05	1.04E-02	10.610	0.968	5.89E-04	1.01E+06
122	0.6096	0.00677	90	0.0	0.00E+00	-0.15	-9.27E+05	10.0	9.42E+05	9.56E-03	9.776	0.935	5.89E-04	1.01E+06
123	0.6096	0.00677	90	0.0	0.00E+00	-0.15	-9.27E+05	15.0	8.97E+05	8.64E-03	8.839	0.891	5.89E-04	1.01E+06
124	0.6096	0.00677	90	0.0	0.00E+00	0.00	0.00E+00	5.0	1.08E+06	1.31E-02	13.386	1.045	5.89E-04	1.03E+06
125	0.6096	0.00677	90	0.0	0.00E+00	0.00	0.00E+00	10.0	1.04E+06	1.15E-02	11.733	1.006	5.89E-04	1.03E+06
126	0.6096	0.00677	90	0.0	0.00E+00	0.00	0.00E+00	15.0	1.01E+06	1.04E-02	10.648	0.977	5.89E-04	1.03E+06
136	0.6096	0.00677	90	0.4	4.33E+06	-0.30	-3.09E+06	5.0	6.27E+05	1.05E-02	3.595	0.638	1.77E-03	9.83E+05
137	0.6096	0.00677	90	0.4	4.33E+06	-0.30	-3.09E+06	10.0	5.89E+05	8.84E-03	3.016	0.599	1.77E-03	9.83E+05
138	0.6096	0.00677	90	0.4	4.33E+06	-0.30	-3.09E+06	15.0	5.56E+05	7.72E-03	2.632	0.566	1.77E-03	9.83E+05
139	0.6096	0.00677	90	0.4	4.33E+06	-0.15	-2.16E+06	5.0	8.18E+05	1.20E-02	4.085	0.753	1.77E-03	1.09E+06
140	0.6096	0.00677	90	0.4	4.33E+06	-0.15	-2.16E+06	10.0	7.77E+05	1.04E-02	3.534	0.715	1.77E-03	1.09E+06
141	0.6096	0.00677	90	0.4	4.33E+06	-0.15	-2.16E+06	15.0	7.38E+05	9.17E-03	3.126	0.679	1.77E-03	1.09E+06
142	0.6096	0.00677	90	0.4	4.33E+06	0.00	-1.24E+06	5.0	9.74E+05	1.40E-02	4.778	0.869	1.77E-03	1.12E+06
143	0.6096	0.00677	90	0.4	4.33E+06	0.00	-1.24E+06	10.0	9.39E+05	1.21E-02	4.122	0.838	1.77E-03	1.12E+06
144	0.6096	0.00677	90	0.4	4.33E+06	0.00	-1.24E+06	15.0	9.07E+05	1.09E-02	3.723	0.809	1.77E-03	1.12E+06
154	0.6096	0.00677	90	0.8	8.67E+06	-0.30	-4.33E+06	5.0	1.47E+05	1.35E-02	2.768	0.248	2.95E-03	5.93E+05
155	0.6096	0.00677	90	0.8	8.67E+06	-0.30	-4.33E+06	10.0	1.44E+05	1.26E-02	2.574	0.243	2.95E-03	5.93E+05
156	0.6096	0.00677	90	0.8	8.67E+06	-0.30	-4.33E+06	15.0	1.30E+05	1.03E-02	2.101	0.219	2.95E-03	5.93E+05
157	0.6096	0.00677	90	0.8	8.67E+06	-0.15	-3.40E+06	5.0	3.92E+05	1.87E-02	3.834	0.508	2.95E-03	7.72E+05
158	0.6096	0.00677	90	0.8	8.67E+06	-0.15	-3.40E+06	10.0	3.75E+05	1.57E-02	3.208	0.486	2.95E-03	7.72E+05
159	0.6096	0.00677	90	0.8	8.67E+06	-0.15	-3.40E+06	15.0	3.65E+05	1.47E-02	2.998	0.473	2.95E-03	7.72E+05
160	0.6096	0.00677	90	0.8	8.67E+06	0.00	-2.47E+06	5.0	6.18E+05	2.16E-02	4.420	0.743	2.95E-03	8.32E+05
161	0.6096	0.00677	90	0.8	8.67E+06	0.00	-2.47E+06	10.0	6.05E+05	1.90E-02	3.887	0.727	2.95E-03	8.32E+05
162	0.6096	0.00677	90	0.8	8.67E+06	0.00	-2.47E+06	15.0	5.84E+05	1.66E-02	3.396	0.702	2.95E-03	8.32E+05

Run Number	Outside Diameter (m)	Wall Thickness (m)	D/t (-)	Beta (-)	Pressure (Pa)	N (-)	Axial Force (N)	Imperfection (% tn)	Critical Moment (Nm)	Critical Curvature (-)	Normalized Strain	Normalized Moment	DNV Strain	DNV Moment
55	0.9144	0.01016	90	0.0	0.00E+00	-0.30	-4.17E+06	5.0	2.81E+06	6.23E-03	9.555	0.898	5.89E-04	3.13E+06
56	0.9144	0.01016	90	0.0	0.00E+00	-0.30	-4.17E+06	10.0	2.60E+06	5.30E-03	8.128	0.831	5.89E-04	3.13E+06
57	0.9144	0.01016	90	0.0	0.00E+00	-0.30	-4.17E+06	15.0	2.48E+06	4.97E-03	7.620	0.793	5.89E-04	3.13E+06
58	0.9144	0.01016	90	0.0	0.00E+00	-0.15	-2.09E+06	5.0	3.32E+06	7.25E-03	11.120	0.977	5.89E-04	3.40E+06
59	0.9144	0.01016	90	0.0	0.00E+00	-0.15	-2.09E+06	10.0	3.14E+06	6.33E-03	9.721	0.924	5.89E-04	3.40E+06
60	0.9144	0.01016	90	0.0	0.00E+00	-0.15	-2.09E+06	15.0	3.02E+06	5.88E-03	9.019	0.889	5.89E-04	3.40E+06
61	0.9144	0.01016	90	0.0	0.00E+00	0.00	0.00E+00	5.0	3.61E+06	8.59E-03	13.177	1.035	5.89E-04	3.49E+06
62	0.9144	0.01016	90	0.0	0.00E+00	0.00	0.00E+00	10.0	3.50E+06	7.80E-03	11.964	1.003	5.89E-04	3.49E+06
63	0.9144	0.01016	90	0.0	0.00E+00	0.00	0.00E+00	15.0	3.39E+06	7.05E-03	10.824	0.972	5.89E-04	3.49E+06
64	0.9144	0.01016	90	0.4	4.33E+06	-0.30	-6.96E+06	5.0	2.10E+06	7.02E-03	3.591	0.633	1.77E-03	3.32E+06
65	0.9144	0.01016	90	0.4	4.33E+06	-0.30	-6.96E+06	10.0	1.97E+06	5.87E-03	3.003	0.594	1.77E-03	3.32E+06
66	0.9144	0.01016	90	0.4	4.33E+06	-0.30	-6.96E+06	15.0	1.88E+06	5.24E-03	2.680	0.567	1.77E-03	3.32E+06
67	0.9144	0.01016	90	0.4	4.33E+06	-0.15	-4.87E+06	5.0	2.77E+06	8.25E-03	4.220	0.755	1.77E-03	3.67E+06
68	0.9144	0.01016	90	0.4	4.33E+06	-0.15	-4.87E+06	10.0	2.59E+06	6.89E-03	3.525	0.706	1.77E-03	3.67E+06
69	0.9144	0.01016	90	0.4	4.33E+06	-0.15	-4.87E+06	15.0	2.49E+06	6.30E-03	3.225	0.679	1.77E-03	3.67E+06
70	0.9144	0.01016	90	0.4	4.33E+06	0.00	-2.78E+06	5.0	3.29E+06	9.62E-03	4.920	0.870	1.77E-03	3.78E+06
71	0.9144	0.01016	90	0.4	4.33E+06	0.00	-2.78E+06	10.0	3.17E+06	8.29E-03	4.238	0.838	1.77E-03	3.78E+06
72	0.9144	0.01016	90	0.4	4.33E+06	0.00	-2.78E+06	15.0	3.04E+06	7.29E-03	3.731	0.803	1.77E-03	3.78E+06
73	0.9144	0.01016	90	0.8	8.67E+06	-0.30	-9.74E+06	5.0	5.12E+05	9.96E-03	3.056	0.256	2.95E-03	2.00E+06
74	0.9144	0.01016	90	0.8	8.67E+06	-0.30	-9.74E+06	10.0	4.82E+05	8.39E-03	2.575	0.241	2.95E-03	2.00E+06
75	0.9144	0.01016	90	0.8	8.67E+06	-0.30	-9.74E+06	15.0	4.42E+05	7.20E-03	2.209	0.221	2.95E-03	2.00E+06
76	0.9144	0.01016	90	0.8	8.67E+06	-0.15	-7.65E+06	5.0	1.31E+06	1.21E-02	3.705	0.503	2.95E-03	2.61E+06
77	0.9144	0.01016	90	0.8	8.67E+06	-0.15	-7.65E+06	10.0	1.26E+06	1.08E-02	3.319	0.483	2.95E-03	2.61E+06
78	0.9144	0.01016	90	0.8	8.67E+06	-0.15	-7.65E+06	15.0	1.19E+06	9.14E-03	2.806	0.457	2.95E-03	2.61E+06
79	0.9144	0.01016	90	0.8	8.67E+06	0.00	-5.56E+06	5.0	2.10E+06	1.53E-02	4.696	0.748	2.95E-03	2.81E+06
80	0.9144	0.01016	90	0.8	8.67E+06	0.00	-5.56E+06	10.0	2.00E+06	1.19E-02	3.652	0.712	2.95E-03	2.81E+06
81	0.9144	0.01016	90	0.8	8.67E+06	0.00	-5.56E+06	15.0	1.96E+06	1.12E-02	3.423	0.698	2.95E-03	2.81E+06

FOR D/t = 90 DNV STRAIN ASSUMES DNV OS-F101 GIRTH WELD FACTOR IS 0.6







